

Performance Analysis of Plug-and-Play ADMM: A Graph Signal Processing Perspective

Stanley H. Chan, *Senior Member, IEEE*

Abstract—The Plug-and-Play (PnP) ADMM algorithm is a powerful image restoration framework that allows advanced image denoising priors to be integrated into physical forward models to generate high quality image restoration results. However, despite the enormous number of applications and several theoretical studies trying to prove the convergence by leveraging tools in convex analysis, very little is known about why the algorithm is doing so well. The goal of this paper is to fill the gap by discussing the performance of PnP ADMM. By restricting the denoisers to the class of graph filters under a linearity assumption, or more specifically the symmetric smoothing filters, we offer three contributions: (1) We show conditions under which an equivalent maximum-a-posteriori (MAP) optimization exists, (2) we present a geometric interpretation and show that the performance gain is due to an intrinsic pre-denoising characteristic of the PnP prior, (3) we introduce a new analysis technique via the concept of consensus equilibrium, and provide interpretations to problems involving multiple priors.

Index Terms—Plug-and-Play ADMM, consensus equilibrium, image restoration, image denoising

I. INTRODUCTION

The Plug-and-Play (PnP) ADMM is a variant of the alternating direction method of multiplier (ADMM) algorithm. Since its introduction in 2013 [1], the algorithm has demonstrated extremely promising results in image restoration and signal recovery problems [2]–[8]. However, despite the enormous number of applications and several studies on its convergence [8]–[10], it is generally unclear why the algorithm is performing so well. On the one hand, one can argue that the superior performance is attributed to the underlying image denoisers, which is evident from applications using convolutional neural networks [11]–[14]. Yet on the other hand, unless we can explicitly write down the optimization, e.g., in the form of maximum-a-posteriori (MAP), it will be extremely difficult to quantify the solution even if we know the solution exists. The goal of this paper is to present a set of analytic results so that we can understand the behavior of PnP ADMM. To do so, we consider a subset of image denoisers known as the graph filters or symmetric smoothing filters. Under such setting, we are able to explicitly show the geometry of the algorithm and make comparison with graph Laplacian based restoration algorithms.

In order to state the problem more concretely, it would be useful to first review the PnP ADMM. The starting point of

the PnP ADMM is the ADMM algorithm, which has become a standard tool for minimizing a sum of two separable functions of the form

$$\hat{\mathbf{x}} = \underset{\mathbf{x}}{\operatorname{argmin}} f(\mathbf{x}) + \lambda g(\mathbf{x}). \quad (1)$$

Here, f represents the *objective function* arising from the physical measurement models, e.g., blur, sampling, projection, or other linear transformations. The function g is the *regularization function*, representing the prior model of the underlying signals, e.g., ℓ_p -norm, sparsity, or total variation. The parameter λ is the regularization constant, and is assumed known a-priori and is fixed in this paper. Problems taking the form of (1) is broad, encompassing various linear inverse problems in imaging, deblurring, super-resolution, CT, MRI, and compressed sensing, to name a few.

The ADMM algorithm solves (1) by converting the unconstrained optimization into a constrained problem

$$(\hat{\mathbf{x}}, \hat{\mathbf{v}}) = \underset{\mathbf{x}, \mathbf{v}}{\operatorname{argmin}} f(\mathbf{x}) + \lambda g(\mathbf{v}), \text{ subject to } \mathbf{x} = \mathbf{v}. \quad (2)$$

It then considers the augmented Lagrangian function:

$$\mathcal{L}(\mathbf{x}, \mathbf{v}, \mathbf{u}) = f(\mathbf{x}) + \lambda g(\mathbf{v}) + \mathbf{u}^T(\mathbf{x} - \mathbf{v}) + \frac{\rho}{2} \|\mathbf{x} - \mathbf{v}\|^2. \quad (3)$$

Then, the algorithm finds the solution by seeking a saddle point of \mathcal{L} , which involves solving a sequence of subproblems in the form

$$\mathbf{x}^{(k+1)} = \underset{\mathbf{x} \in \mathbb{R}^n}{\operatorname{argmin}} f(\mathbf{x}) + \frac{\rho}{2} \|\mathbf{x} - \tilde{\mathbf{x}}^{(k)}\|^2, \quad (4)$$

$$\mathbf{v}^{(k+1)} = \underset{\mathbf{v} \in \mathbb{R}^n}{\operatorname{argmin}} \lambda g(\mathbf{v}) + \frac{\rho}{2} \|\mathbf{v} - \tilde{\mathbf{v}}^{(k)}\|^2, \quad (5)$$

$$\bar{\mathbf{u}}^{(k+1)} = \bar{\mathbf{u}}^{(k)} + (\mathbf{x}^{(k+1)} - \mathbf{v}^{(k+1)}), \quad (6)$$

where $\bar{\mathbf{u}}^{(k)} \stackrel{\text{def}}{=} (1/\rho)\mathbf{u}^{(k)}$ is the scaled Lagrange multiplier, $\tilde{\mathbf{x}}^{(k)} \stackrel{\text{def}}{=} \mathbf{v}^{(k)} - \bar{\mathbf{u}}^{(k)}$ and $\tilde{\mathbf{v}}^{(k)} \stackrel{\text{def}}{=} \mathbf{x}^{(k+1)} + \bar{\mathbf{u}}^{(k)}$ are the intermediate variables. Under mild conditions, e.g., when both f and g are closed, proper and convex, and if a saddle point of \mathcal{L} exists, one can show that the iterates returned by (4)–(6) converges to the solution of (1). Readers interested in knowing more about the theoretical properties of ADMM can consult tutorials such as [15].

The idea of PnP ADMM is to modify (5) by observing that it is a denoising step if we treat $\tilde{\mathbf{v}}^{(k)}$ as a “noisy” version of \mathbf{v} and $g(\mathbf{v})$ as a regularization for \mathbf{v} . Based on this, we can replace (5) by a denoiser $\mathcal{D}_\sigma : \mathbb{R}^n \rightarrow \mathbb{R}^n$ such that

$$\mathbf{v}^{(k+1)} = \mathcal{D}_\sigma \left(\tilde{\mathbf{v}}^{(k)} \right), \quad (7)$$

where $\sigma = \sqrt{\lambda/\rho}$ is the denoising strength or a hypothesized

“noise level”. The choice of \mathcal{D}_σ is broad. \mathcal{D}_σ can be a proximal map such as total variation denoising, or an off-the-shelf image denoisers such as BM3D, non-local means, and more recently neural networks.

Replacing the explicit optimization in (5) by an off-the-shelf denoiser in (7) leads to many interesting questions:

- **Existence of g .** Given an arbitrary denoiser \mathcal{D}_σ , is it possible to have an equivalent g such that (5) and (7) coincide? If not, under what conditions of \mathcal{D}_σ would this happen? Some recent studies provide an answer, e.g., [8], [10], [16], which will be elaborated in later sections of this paper. An alternative approach is the Regularization by Denoising (RED) [17], which has advantages and limitations. Other variations include [10], [18], [19].
- **Convergence.** Does PnP ADMM converge? Majority of the known results are based on a classical result of Moreau [20], which suggests that global convergence of PnP ADMM is guaranteed if and only if \mathcal{D}_σ has symmetric gradient and is non-expansive (See [8] and [10]). However, non-expansiveness and symmetric gradient are strong conditions that do not hold for all denoisers. A relaxed criteria by fixed point convergence allows one to prove convergence for a slightly broader class of denoisers which are asymptotically invariant as $\sigma \rightarrow 0$ [9]. Fixed point convergence does not guarantee converging to a solution of certain optimization (because such optimization may not even exist), yet practically the fixed point can correspond to a meaningful image when the parameters are set properly.
- **Performance.** If g does exist, what is it and why is it an effective regularization function? An earlier work of Chan showed the form of g for symmetric smoothing filters [21], and a similar result is recently reported by [10]. We will elaborate more on this later. If g does not exist, it would be important to know what does PnP ADMM solve, and why it is good. The focus of this paper is to address this performance issue. We will take two paths, one through the MAP formulation, and the other one through a concept called the consensus equilibrium.
- **Generalization.** How to generalize the algorithm to multiple denoisers? The generalization can be done by a technique called consensus equilibrium [22]. However, can we explain the performance, and how to determine the optimal combination weights?

To enable our study, we assume that the denoisers are in the family of symmetric smoothing filters [23]–[25] or graph filters [26]–[32]. These filters are simple in the sense that they are (pseudo) linear and hence they can be expressed using matrices. However, they are also representative enough to cover a sufficiently large group of image denoisers that we encounter in the literature.

The remaining of the paper is arranged as follows. We begin with a brief review of the construction of graph filters and their properties in Section 2. The main results are presented in Section 3 and 4. Section 3 analyzes the problem from a MAP perspective, whereas Section 4 approaches the problem from the consensus equilibrium perspective. Further discussions of

open problems are presented in Section 5.

II. GRAPH FILTERS

A. Constructing a Graph Filter

Graph filter is a class of linear denoisers originally developed in the area of graph signal processing. The application of graph filters is very broad, e.g., deblurring using graph Laplacian [29], boosting image denoisers [27], image denoising using global similarity [30], JPEG compression using random walk [33], and blind deconvolution using reweighted graph total variation [32]. In terms of theory, there are studies of the graphs in continuous domain [31], sampling of graphs [34], and filter banks of graphs [35], to name a few.

Represented as matrices, graph filters take the form of

$$\hat{\mathbf{x}} = \mathcal{D}_\sigma(\mathbf{y}) = \mathbf{W}\mathbf{y}. \quad (8)$$

We call the matrix $\mathbf{W} \in \mathbb{R}^{n \times n}$ a graph filter. There are multiple ways of constructing \mathbf{W} . One of the most commonly used approaches is to define a non-local weight kernel $\mathbf{K} \in \mathbb{R}^{n \times n}$:

$$[\mathbf{K}]_{ij} = \exp \left\{ -\frac{\|\mathbf{y}_i - \mathbf{y}_j\|^2}{2h^2} \right\}, \quad (9)$$

where $\mathbf{y}_i \in \mathbb{R}^d$ is a d -dimensional patch centered at pixel i , and h is a parameter characterizing the denoising strength of the filter. Modifications to (9) are common, e.g., by incorporating spatial distance (which gives the non-local means filter), restricting to pixels instead of patches (which gives the bilateral filter), or extending the norm to a weighted norm (which gives the kernel regression filter). For more examples of the kernel matrices, we refer the readers to [23].

The \mathbf{K} matrix defined in (9) is symmetric but the row sum $\mathbf{K}\mathbf{1}$ is not 1. Thus, \mathbf{K} cannot be used directly as a denoising filter because it amplifies or attenuates signals. To normalize the matrix while preserving the symmetry, one can apply the Sinkhorn-Knopp balancing algorithm [24], [25], [36] to iteratively normalizes the rows and columns of \mathbf{K} until convergence. When \mathbf{K} is symmetrized, the resulting matrix is called a symmetric smoothing filter, given by

$$\mathbf{W} = \mathbf{D}^{-1/2} \mathbf{K} \mathbf{D}^{-1/2}, \quad (10)$$

where the diagonal matrix \mathbf{D} is defined such that $\mathbf{W}\mathbf{1} = \mathbf{1}$ and $\mathbf{W}^T \mathbf{1} = \mathbf{1}$. Since the columns and rows of \mathbf{W} sum to 1, \mathbf{W} is a *symmetric doubly stochastic matrix*. It has been observed that the symmetrized \mathbf{W} in (10) has a better denoising performance than its non-symmetric counterpart $\tilde{\mathbf{W}} = \tilde{\mathbf{D}}^{-1} \mathbf{K}$ where $\tilde{\mathbf{D}} = \text{diag}(\mathbf{K}\mathbf{1})$. This is attributed to the implicit clustering of the pixels during the Sinkhorn-Knopp balancing algorithm [25], among other reasons such as reduced degree of freedom so that the drop in variance overrides the gain in bias [24].

B. Properties of Graph Filters

Properties. The graph filter \mathbf{W} has a number of properties. We list a few of them here.

- \mathbf{W} can be considered as a weighted adjacency matrix of an undirected graph. The (i, j) -th element $[\mathbf{W}]_{ij}$ is the weight on the edge linking node i and node j .

- $0 \leq \lambda_n(\mathbf{W}) \leq \dots \leq \lambda_1(\mathbf{W}) = 1$. This follows from the fact that \mathbf{W} is doubly stochastic, and so the eigenvalues are all non-negative.
- $\mathbf{I} - \mathbf{W}$ is the graph Laplacian, with the zero eigenvalue associated to the vector $\frac{1}{\sqrt{n}}\mathbf{1}$.
- The regularization defined through the graph Laplacian $\mathbf{x}^T(\mathbf{I} - \mathbf{W})\mathbf{x}$ can be interpreted as

$$\mathbf{x}^T(\mathbf{I} - \mathbf{W})\mathbf{x} = \sum_{i=1}^n \sum_{j \neq i}^n [\mathbf{K}]_{ij} \left(\frac{x_i}{\sqrt{[\mathbf{D}]_{ii}}} - \frac{x_j}{\sqrt{[\mathbf{D}]_{jj}}} \right)^2, \quad (11)$$

which is measuring the smoothness of the signal \mathbf{x} with the weights defined by the graph \mathbf{W} .

To analyze the spectral property of \mathbf{W} , we consider the eigen-decomposition $\mathbf{W} = \mathbf{U}\mathbf{S}\mathbf{U}^T$ where \mathbf{U} is the eigenvector matrix and \mathbf{S} is the eigenvalue matrix. If \mathbf{W} is not invertible, i.e., $\text{rank}(\mathbf{W}) = r < n$, we can further decompose \mathbf{W} into

$$\mathbf{W} = [\mathbf{U}_1 \quad \mathbf{U}_2] \begin{bmatrix} \mathbf{S}_1 & \\ & \mathbf{S}_2 \end{bmatrix} \begin{bmatrix} \mathbf{U}_1^T \\ \mathbf{U}_2^T \end{bmatrix}, \quad (12)$$

where $\mathbf{S}_2 = \mathbf{0}$, and $\mathbf{S}_1 \in \mathbb{R}^{r \times r}$ is a diagonal matrix storing the non-zero eigenvalues of \mathbf{W} . Since $\mathbf{S}_2 = \mathbf{0}$, we can simplify \mathbf{W} as $\mathbf{W} = \mathbf{U}_1 \mathbf{S}_1 \mathbf{U}_1^T$.

Pseudo-Linearity. In the actual PnP ADMM implementation, \mathbf{W} is pseudo-linear rather than linear. That is, the matrix \mathbf{W} is a function of the input noisy image \mathbf{y} , or more precisely $\hat{\mathbf{x}} = \mathbf{W}(\mathbf{y})\mathbf{y}$ instead of (8). However, as mentioned in [37], the dependency of \mathbf{W} on \mathbf{y} is typically small if \mathbf{W} is estimated from a *pre-filtered* version of \mathbf{y} , for example applying a baseline denoising algorithm to \mathbf{y} and constructing a new weight matrix \mathbf{W} based on the baseline estimate. In practice, using a fixed \mathbf{W} is justified in applications such as [8], where \mathbf{W} is updated for the first tens of iterations and is kept fixed for the remaining iterations. Following the same line of arguments, we assume that \mathbf{W} is pre-defined and is independent of \mathbf{y} . We will occasionally look at the *oracle* case where \mathbf{W} is estimated from the ground truth \mathbf{x} so that we can quantify the *best possible* performance of the algorithm. But in general we only require that \mathbf{W} is independent of \mathbf{y} .

Energy Concentration. When applied to a noisy signal \mathbf{y} , \mathbf{W} projects \mathbf{y} onto the space spanned by its columns. The effectiveness of this projection is determined by how well \mathbf{W} is generated. In the oracle setting where \mathbf{W} is generated from the ground truth signal \mathbf{x} , the first few eigenvectors of \mathbf{W} is sufficient to capture most of the energy of \mathbf{x} and leaving the noise in the remaining eigenvectors. This is illustrated in the Figure 1, where we consider a 1D signal \mathbf{x} and its noisy version \mathbf{y} . The weight matrix \mathbf{W} is constructed from the ground truth \mathbf{x} using a non-local means kernel defined in (9). By projecting \mathbf{x} and \mathbf{y} using the eigenvector matrix \mathbf{U} , we see that $\mathbf{U}^T \mathbf{x}$ has significantly fewer non-zeros than $\mathbf{U}^T \mathbf{y}$ for large eigen-indices.

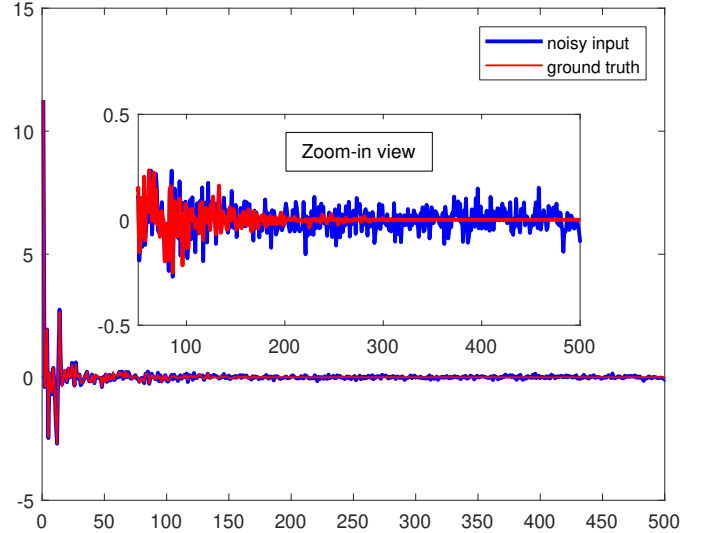


Fig. 1. Projecting a noisy signal \mathbf{y} and the ground truth signal \mathbf{x} by the principle eigenvectors. The two curves show $\mathbf{U}^T \mathbf{y}$ and $\mathbf{U}^T \mathbf{x}$, where \mathbf{U} is the eigenvector matrix of \mathbf{W} .

III. PERFORMANCE ANALYSIS VIA MAP

In this section we present the first set of analytic results. We call it the maximum-a-posteriori (MAP) analysis because we need to explicitly derive the MAP optimization.

A. Existence of g

Given an arbitrary denoiser $\mathcal{D}_\sigma : \mathbb{R}^n \rightarrow \mathbb{R}^n$, the question we ask is whether it is possible to obtain a regularization function g defined in (5). One way to answer this question is to use a property of the proximal operator by Moreau [20] and show that \mathcal{D}_σ corresponds to a proximal map with a convex g , a result previously used by Sreehari *et al.* [8] and more recently by Teodoro *et al.* [10].

Lemma 1 (Moreau [20]). *A denoiser $\mathcal{D}_\sigma : \mathbb{R}^n \rightarrow \mathbb{R}^n$ is the proximal map of some function if and only if*

- \mathcal{D}_σ is non-expansive, i.e., $\|\mathcal{D}_\sigma(\mathbf{x}) - \mathcal{D}_\sigma(\mathbf{y})\| \leq \|\mathbf{x} - \mathbf{y}\|$ for any \mathbf{x} and \mathbf{y} , and
- \mathcal{D}_σ is a sub-gradient of some convex function, i.e., there exists φ such that $\mathcal{D}_\sigma(\mathbf{x}) \in \partial\varphi(\mathbf{x})$.

An immediate implication of Lemma 1 is that if \mathcal{D}_σ is continuously differentiable, then the subgradient $\partial\varphi$ reduces to the gradient $\nabla\varphi$. Reehorst and Schniter [16] use a classical result by Kantorovitz [38] (in particular Theorem 4.3.8 and 4.3.10) to argue that for such φ to exist, \mathcal{D}_σ must have a symmetric Jacobian. Therefore, symmetry is necessary for φ to exist. Note, however, that symmetry is not sufficient. If \mathcal{D}_σ does not have a symmetric Jacobian, then φ certainly does not exist. But if \mathcal{D}_σ has a symmetric Jacobian, one cannot conclude that φ must exist.

Under the context of symmetric smoothing filters, i.e., $\mathcal{D}_\sigma(\mathbf{x}) = \mathbf{W}\mathbf{x}$, both conditions of the Moreau Lemma are satisfied: Non-expansiveness is given by the fact that $\lambda_1(\mathbf{W}) \leq 1$, and the sub-gradient condition holds because $\mathcal{D}_\sigma(\mathbf{x}) = \mathbf{W}\mathbf{x} = \nabla\varphi(\mathbf{x})$ where $\varphi(\mathbf{x}) = \frac{1}{2}\mathbf{x}^T \mathbf{W}\mathbf{x}$.

B. Deriving g

We can now derive an explicit form of g when $\mathcal{D}_\sigma(\mathbf{x}) = \mathbf{W}\mathbf{x}$. We will start with a special case where \mathbf{W}^{-1} exist. The first appearance of this result was reported by Chan [21], and recently generalized by Teodoro *et al.* [10]. The proof below is a constructive one, in the sense that we will derive g from \mathcal{D}_σ rather than verifying a given expression of g .

Theorem 1. *Let $\mathbf{W} \in \mathbb{R}^{n \times n}$ be a graph filter, and assume that \mathbf{W}^{-1} exists. Define $g : \mathbb{R}^n \rightarrow \mathbb{R}$ as*

$$g(\mathbf{x}) = \frac{1}{2\sigma^2} \mathbf{x}^T (\mathbf{W}^{-1} - \mathbf{I}) \mathbf{x}. \quad (13)$$

Then the solution of the minimization of (5) is

$$\hat{\mathbf{x}} \stackrel{\text{def}}{=} \underset{\mathbf{x} \in \mathbb{R}^n}{\text{argmin}} g(\mathbf{x}) + \frac{1}{2\sigma^2} \|\mathbf{x} - \tilde{\mathbf{x}}\|^2 = \mathbf{W}\tilde{\mathbf{x}}. \quad (14)$$

Proof. The existence of g is guaranteed by the Moreau Lemma. Taking the gradient of the objective function of (14) and equating to zero yields $\nabla g(\mathbf{x}) + \frac{1}{\sigma^2}(\mathbf{x} - \tilde{\mathbf{x}}) = \mathbf{0}$, which is equivalent to

$$(\mathbf{I} + \sigma^2 \nabla g)(\mathbf{x}) = \tilde{\mathbf{x}}. \quad (15)$$

Define $\mathbf{G} \in \mathbb{R}^{n \times n}$ as the matrix representation of ∇g such that $\mathbf{G}\mathbf{x} = \nabla g(\mathbf{x})$. Then (15) can be simplified as $(\mathbf{I} + \sigma^2 \mathbf{G})\mathbf{x} = \tilde{\mathbf{x}}$. Substituting $\mathbf{x} = \mathbf{W}\tilde{\mathbf{x}}$, we have that $(\mathbf{I} + \sigma^2 \mathbf{G})\mathbf{W}\tilde{\mathbf{x}} = \tilde{\mathbf{x}}$. Since this result holds for any $\tilde{\mathbf{x}}$, we have $(\mathbf{I} + \sigma^2 \mathbf{G})\mathbf{W} = \mathbf{I}$, which implies that $\mathbf{G} = \frac{1}{\sigma^2}(\mathbf{W}^{-1} - \mathbf{I})$. Therefore,

$$\nabla g(\mathbf{x}) = \mathbf{G}\mathbf{x} = \frac{1}{\sigma^2}(\mathbf{W}^{-1} - \mathbf{I})\mathbf{x}. \quad (16)$$

Integrating both sides yields $g(\mathbf{x}) = \frac{1}{2} \mathbf{x}^T \mathbf{G}\mathbf{x}$. \square

If \mathbf{W} is not invertible, the function $g(\mathbf{x})$ should be

$$g(\mathbf{x}) = \frac{1}{2\sigma^2} \mathbf{x}^T \mathbf{U}_1 (\mathbf{S}_1^{-1} - \mathbf{I}) \mathbf{U}_1^T \mathbf{x} + \iota_\Omega(\mathbf{x}), \quad (17)$$

where ι_Ω denotes an indicator function such that $\iota_\Omega(\mathbf{x}) = 0$ if $\mathbf{x} \in \Omega$ and $\iota_\Omega(\mathbf{x}) = +\infty$ if $\mathbf{x} \notin \Omega$, and the set Ω is defined as $\Omega = \{\mathbf{x} \mid \mathbf{U}_2^T \mathbf{x} = \mathbf{0}\}$. An intuitive argument is that $\mathbf{x}^T (\mathbf{W}^{-1} - \mathbf{I}) \mathbf{x}$ can be (symbolically) written as

$$\begin{aligned} \mathbf{x}^T (\mathbf{W}^{-1} - \mathbf{I}) \mathbf{x} &= \mathbf{x}^T \mathbf{U}_1 (\mathbf{S}_1^{-1} - \mathbf{I}) \mathbf{U}_1^T \mathbf{x} + \\ &+ \mathbf{x}^T \mathbf{U}_2 (\mathbf{S}_2^{-1} - \mathbf{I}) \mathbf{U}_2^T \mathbf{x}. \end{aligned} \quad (18)$$

If we put $\mathbf{S}_2^{-1} = \infty$, then minimizing $\mathbf{x}^T (\mathbf{W}^{-1} - \mathbf{I}) \mathbf{x}$ will force $\mathbf{U}_2^T \mathbf{x} = \mathbf{0}$ if we do not allow the trivial solution $\mathbf{x} = \mathbf{0}$. In this case, the function g becomes the one shown in (17).

To formally prove the result, we substitute (17) into (14) and check if the optimality condition in (15) is satisfied, i.e.,

$$(\mathbf{I} + \sigma^2 \mathbf{G})\mathbf{W}\mathbf{x} = \mathbf{x}, \quad (19)$$

for any \mathbf{x} . Clearly, if $\mathbf{x} \notin \Omega$, then $g(\mathbf{x})$ in (17) is unbounded and so (14) does not have a solution. However, if $\mathbf{x} \in \Omega$, then we can write $\mathbf{W} = \mathbf{U}_1 \mathbf{S}_1 \mathbf{U}_1^T$ and substitute $\mathbf{G} = \frac{1}{\sigma^2} \mathbf{U}_1 (\mathbf{S}_1^{-1} - \mathbf{I}) \mathbf{U}_1^T$ into (19). This will give us

$$\begin{aligned} (\mathbf{I} + \sigma^2 \mathbf{G})\mathbf{W}\mathbf{x} &= (\mathbf{I} + \mathbf{U}_1 (\mathbf{S}_1^{-1} - \mathbf{I}) \mathbf{U}_1^T) (\mathbf{U}_1 \mathbf{S}_1 \mathbf{U}_1^T) \mathbf{x} \\ &= \mathbf{U}_1 \mathbf{S}_1 \mathbf{U}_1^T \mathbf{x} + \mathbf{U}_1 (\mathbf{I} - \mathbf{S}_1) \mathbf{U}_1^T \mathbf{x} \\ &= \mathbf{x}. \end{aligned}$$

Therefore, if $\mathbf{x} \in \Omega$, the optimality condition in (15) is satisfied. The non-invertible case has interesting implications which we shall discuss further in Section III.F.

C. The Role of ρ

One property we like to investigate is the parameter ρ . By substituting (13) into (2), and recalling $\sigma \stackrel{\text{def}}{=} \sqrt{\lambda/\rho}$, we can show that PnP ADMM is solving

$$\underset{\mathbf{x}}{\text{minimize}} f(\mathbf{x}) + \frac{\rho}{2} \mathbf{x}^T (\mathbf{W}^{-1} - \mathbf{I}) \mathbf{x}. \quad (20)$$

In the literature of graph signal processing, the prior in (20) is reminiscent to the classical graph Laplacian. An image restoration using graph Laplacian is

$$\underset{\mathbf{x}}{\text{minimize}} f(\mathbf{x}) + \frac{\lambda}{2} \mathbf{x}^T (\mathbf{I} - \mathbf{W}) \mathbf{x}. \quad (21)$$

An interesting observation here is that in (20), the original regularization parameter λ is eliminated because g contains its reciprocal. Thus, λ is replaced by the ADMM internal parameter ρ . This internal parameter ρ has no influence to the final solution in the classical ADMM because ADMM converges for all ρ when f and g are closed, proper and convex. However, in PnP ADMM, the optimization cost is characterized by ρ . Thus, the solution changes with ρ , a phenomenon reported in earlier papers, e.g., [9].

We can also ask: For the best ρ and λ , how would the solutions of (20) and (21) behave? Figure 2 shows an experimental result where we chose the forward model to be $f(\mathbf{x}) = \frac{1}{2} \|\mathbf{A}\mathbf{x} - \mathbf{y}\|^2$, where the matrix \mathbf{A} is a convolution matrix constructed from a 3-tap filter $[1, 6, 1]/8$. The specific choice of this 3-tap filter is unimportant. (In MATLAB this is $\mathbf{A} = \text{toeplitz}([1 \ 6 \ 1 \ \text{zeros}(1, n-3)])/8$.) The noisy signal \mathbf{y} is one column of the cameraman image, corrupted by i.i.d. Gaussian noise with $\sigma_\eta = 0.05$. (We assume $\mathbf{x} \in [0, 1]$.) The graph filter \mathbf{W} is defined by using a non-local mean kernel matrix \mathbf{K} with $[\mathbf{K}]_{ij} = \exp\{-((i-j)^2/(2h_s^2))\} \exp\{-\|\mathbf{x}_i - \mathbf{x}_j\|^2/(2h_r^2)\}$, which is an oracle case. The patch size is $d = 5$. The parameters are set as $h_s = 5$ and $h_r = 0.1$. Sinkhorn-Knopp symmetrization is applied to make sure \mathbf{W} is symmetric doubly stochastic.

We vary ρ (and equivalently λ) to evaluate the mean squared error (MSE) for a fixed oracle \mathbf{W} . As shown in Figure 2, PnP ADMM and graph Laplacian have different operating regimes for ρ and λ . PnP ADMM prefers smaller ρ , whereas graph Laplacian prefers larger λ . We will explain this observation in Section 4 using the equilibrium analysis.

D. MSE Analysis for Linear Problems

To quantify the performance of PnP, we consider a typical linear inverse problem with a data fidelity term

$$f(\mathbf{x}) = \frac{1}{2} \|\mathbf{A}\mathbf{x} - \mathbf{y}\|^2. \quad (22)$$

Ideally, we like to analyze the performance of PnP for an arbitrary \mathbf{A} . However, if \mathbf{A} is completely arbitrary, the MSE analysis below will involve evaluating eigenvalues of a sum of two Hermitian matrices. There are some classical results

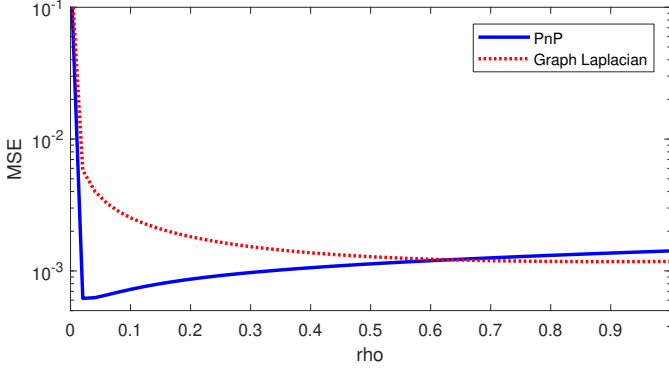


Fig. 2. Mean squared error of the solutions of (20) and (21) as ρ (or λ) increases. PnP has a lower MSE than graph Laplacian for the best ρ and λ .

on bounding the largest and smallest eigenvalues, e.g., [39]. However, finding the exact eigenvalues of a sum of two Hermitian matrices is an open mathematical problem and currently there is no simple solution [40].

In order to ensure analytic tractability, we assume that \mathbf{A} shares the same eigenvector with \mathbf{W} . That is, \mathbf{A} has an eigen-decomposition $\mathbf{A} = \mathbf{U}\mathbf{\Lambda}\mathbf{U}^T$, where \mathbf{U} is also the eigenvector of \mathbf{W} . This is summarized in the following assumption.

Assumption 1. We assume that \mathbf{A} and \mathbf{W} share the same eigenvector, i.e.,

$$\mathbf{A} = \mathbf{U}\mathbf{\Lambda}\mathbf{U}^T, \quad \text{and} \quad \mathbf{W} = \mathbf{U}\mathbf{S}\mathbf{U}^T, \quad (23)$$

where $\mathbf{\Lambda} = \text{diag}(\alpha_1, \dots, \alpha_n)$ and $\mathbf{S} = \text{diag}(s_1, \dots, s_n)$, with $0 \leq \alpha_i \leq 1$ and $0 \leq s_i \leq 1$ for $i = 1, \dots, n$.

While Assumption 1 is strong, it is reasonable to some extent. If we let \mathbf{U} be the Fourier transform matrix, then \mathbf{A} is a convolution matrix representing a blur operation. The corresponding \mathbf{W} is a lowpass filter. If \mathbf{U} is the eigenvector of a graph, or graph Fourier transform [41], then \mathbf{A} can be chosen as a filtering operation in the graph domain, e.g., diffusion over the graph. As a special case, if we assume $\mathbf{\Lambda} = \mathbf{I}$, then \mathbf{A} is simplified to $\mathbf{A} = \mathbf{I}$, which is a denoising problem.

The problem we are interested in studying is the comparison between the PnP formulation and the graph Laplacian formulation:

$$\hat{\mathbf{x}}_L = \underset{\mathbf{x}}{\text{argmin}} \quad \frac{1}{2} \|\mathbf{A}\mathbf{x} - \mathbf{y}\|^2 + \frac{\lambda}{2} \mathbf{x}^T (\mathbf{I} - \mathbf{W})\mathbf{x}, \quad (24)$$

$$\hat{\mathbf{x}}_P = \underset{\mathbf{x}}{\text{argmin}} \quad \frac{1}{2} \|\mathbf{A}\mathbf{x} - \mathbf{y}\|^2 + \frac{\rho}{2} \mathbf{x}^T (\mathbf{W}^{-1} - \mathbf{I})\mathbf{x}. \quad (25)$$

Here, \mathbf{W}^{-1} is only a short-hand notation of the g defined in (17). In the MSE analysis below we will set the eigenvalues to zero if \mathbf{W} is not invertible.

The solutions of the above two problems are respectively

$$\hat{\mathbf{x}}_L = \left[(\mathbf{A}^T \mathbf{A} + \lambda \mathbf{I}) - \lambda \mathbf{W} \right]^{-1} \mathbf{A}^T \mathbf{y} \stackrel{\text{def}}{=} \mathbf{Q}_L^{-1} \mathbf{A}^T \mathbf{y}, \quad (26)$$

$$\hat{\mathbf{x}}_P = \left[(\mathbf{A}^T \mathbf{A} - \rho \mathbf{I}) + \rho \mathbf{W}^{-1} \right]^{-1} \mathbf{A}^T \mathbf{y} \stackrel{\text{def}}{=} \mathbf{Q}_P^{-1} \mathbf{A}^T \mathbf{y}, \quad (27)$$

where the matrices

$$\mathbf{Q}_L \stackrel{\text{def}}{=} (\mathbf{A}^T \mathbf{A} + \lambda \mathbf{I}) - \lambda \mathbf{W}$$

$$\mathbf{Q}_P \stackrel{\text{def}}{=} (\mathbf{A}^T \mathbf{A} - \rho \mathbf{I}) + \rho \mathbf{W}^{-1}$$

are used to simplify notations. Letting $\mathbf{b} \stackrel{\text{def}}{=} \mathbf{U}^T \mathbf{x}$ be the projection of \mathbf{x} by \mathbf{U} , the MSE of $\hat{\mathbf{x}}_L$ is

$$\begin{aligned} \text{MSE}_L &= \mathbb{E} \|\hat{\mathbf{x}}_L - \mathbf{x}\|^2 = \mathbb{E} \|\mathbf{Q}_L^{-1} \mathbf{A}^T (\mathbf{x} + \boldsymbol{\eta}) - \mathbf{x}\|^2 \\ &= \|(\mathbf{Q}_L^{-1} \mathbf{A}^T - \mathbf{I})\mathbf{x}\|^2 + \sigma_\eta^2 \text{Tr} \left[\mathbf{A}^T \left(\mathbf{Q}_L^T \mathbf{Q}_L \right)^{-1} \mathbf{A} \right] \\ &= \sum_{i=1}^n \left(\frac{\alpha_i}{\alpha_i^2 + \lambda - \lambda s_i} - 1 \right)^2 b_i^2 + \sigma_\eta^2 \left(\frac{\alpha_i}{\alpha_i^2 + \lambda - \lambda s_i} \right)^2 \\ &= \sum_{i=1}^n \frac{(\alpha_i^2 + \lambda - \lambda s_i - \alpha_i)^2 b_i^2 + \sigma_\eta^2 \alpha_i^2}{(\alpha_i^2 + \lambda - \lambda s_i)^2}, \end{aligned} \quad (28)$$

and the MSE of $\hat{\mathbf{x}}_P$ is

$$\begin{aligned} \text{MSE}_P &= \mathbb{E} \|\hat{\mathbf{x}}_P - \mathbf{x}\|^2 = \mathbb{E} \|\mathbf{Q}_P^{-1} \mathbf{A}^T (\mathbf{x} + \boldsymbol{\eta}) - \mathbf{x}\|^2 \\ &= \|(\mathbf{Q}_P^{-1} \mathbf{A}^T - \mathbf{I})\mathbf{x}\|^2 + \sigma_\eta^2 \text{Tr} \left[\mathbf{A}^T \left(\mathbf{Q}_P^T \mathbf{Q}_P \right)^{-1} \mathbf{A} \right] \\ &= \sum_{i=1}^n \left(\frac{\alpha_i s_i}{\alpha_i^2 s_i - \rho s_i + \rho} - 1 \right)^2 b_i^2 + \sigma_\eta^2 \left(\frac{\alpha_i s_i}{\alpha_i^2 s_i - \rho s_i + \rho} \right)^2 \\ &= \sum_{i=1}^n \frac{(\alpha_i^2 s_i - \rho s_i + \rho - \alpha_i s_i)^2 b_i^2 + \sigma_\eta^2 \alpha_i^2 s_i^2}{(\alpha_i^2 s_i - \rho s_i + \rho)^2}. \end{aligned} \quad (29)$$

Given \mathbf{A} , \mathbf{W} , \mathbf{x} , ρ and λ , in principle we can completely determine MSE_L and MSE_P . However, instead of resorting to numerical approaches, we analyze the MSEs by looking at the individual terms in the summations above. To this end, we define the i -th term as

$$\text{MSE}_L^i \stackrel{\text{def}}{=} \frac{(\alpha_i^2 + \lambda - \lambda s_i - \alpha_i)^2 b_i^2 + \sigma_\eta^2 \alpha_i^2}{(\alpha_i^2 + \lambda - \lambda s_i)^2}, \quad (30)$$

$$\text{MSE}_P^i \stackrel{\text{def}}{=} \frac{(\alpha_i^2 s_i - \rho s_i + \rho - \alpha_i s_i)^2 b_i^2 + \sigma_\eta^2 \alpha_i^2 s_i^2}{(\alpha_i^2 s_i - \rho s_i + \rho)^2}. \quad (31)$$

When \mathbf{W} is ill-conditioned so that $s_i \rightarrow 0$, we can show that

$$\lim_{s_i \rightarrow 0} \text{MSE}_L^i = \frac{(\alpha_i^2 + \lambda - \alpha_i)^2 b_i^2 + \sigma_\eta^2 \alpha_i^2}{(\alpha_i^2 + \lambda)^2}, \quad (32)$$

$$\lim_{s_i \rightarrow 0} \text{MSE}_P^i = b_i^2. \quad (33)$$

If, in addition to $s_i \rightarrow 0$, we also assume that $b_i \rightarrow 0$ (which typically holds according to the energy concentration of \mathbf{W} demonstrated in Figure 1), then the MSEs become

$$\lim_{b_i, s_i \rightarrow 0} \text{MSE}_L^i = \frac{\sigma_\eta^2 \alpha_i^2}{(\lambda + \alpha_i^2)^2}, \quad \text{and} \quad \lim_{b_i, s_i \rightarrow 0} \text{MSE}_P^i = 0.$$

This shows that the PnP regularization ensures the MSE goes to zero at high frequency (i.e., large eigen-index i) whereas the graph Laplacian has residue MSE at high frequency.

Our next goal is to analyze the bias and variance so that we can understand the composition of the MSE. A typical breakdown of bias and variance is shown in Figure 3.

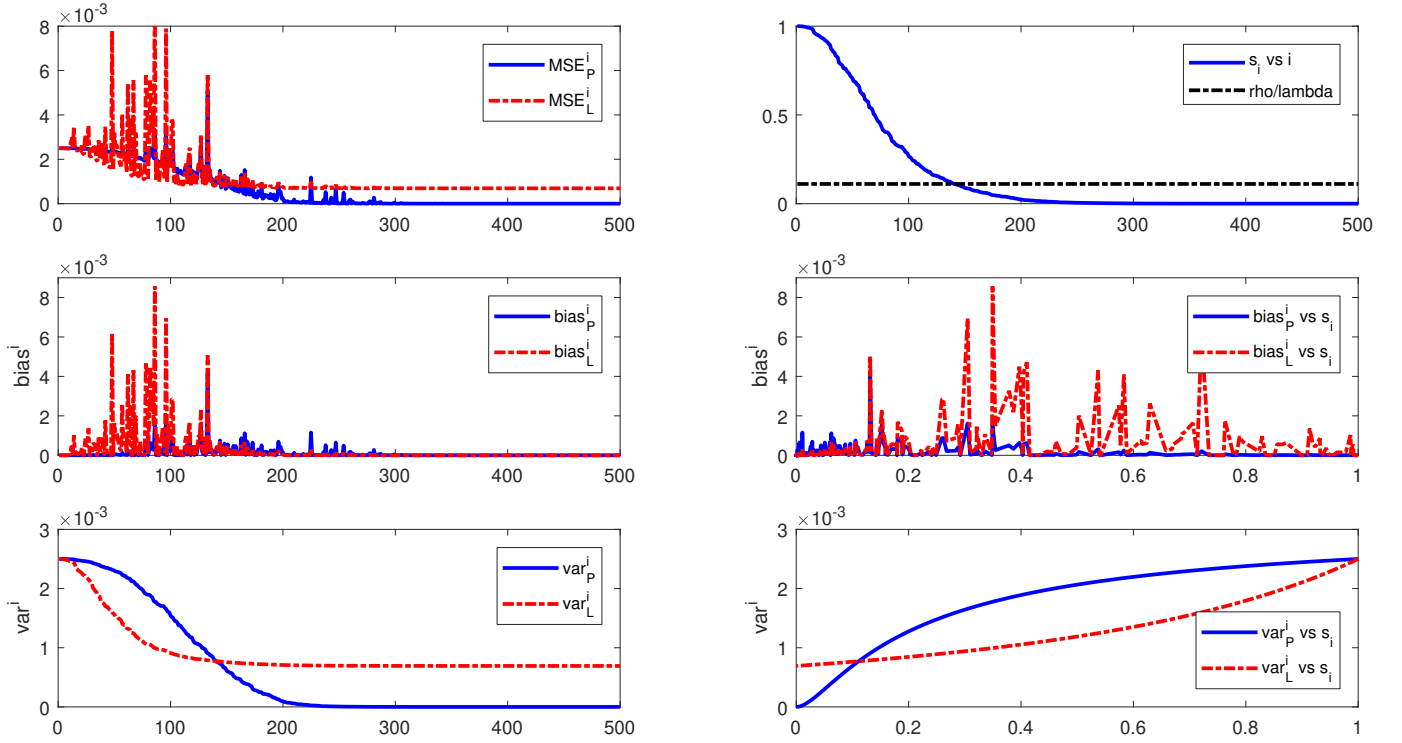


Fig. 3. Bias and variance of PnP and graph Laplacian. The experiment is based on $\mathbf{A} = \mathbf{I}$, $\rho = 0.1$ and $\lambda = 0.9$. The plots on the left show the MSE, bias and variance as a function of the eigen-index i . The top right plot shows the eigenvalue s_i as a function of the eigen-index i . The two plots on the bottom right show the bias and variance as a function of the eigenvalue s_i .

The biases of the two methods are

$$\begin{aligned} \text{Bias}_L^i &= \frac{(\alpha_i^2 + \lambda - \lambda s_i - \alpha_i)^2 b_i^2}{(\alpha_i^2 + \lambda - \lambda s_i)^2}, \\ \text{Bias}_P^i &= \frac{(\alpha_i^2 s_i - \rho s_i + \rho - \alpha_i s_i)^2 b_i^2}{(\alpha_i^2 s_i - \rho s_i + \rho)^2}. \end{aligned} \quad (34)$$

Proposition 1. Assume $\mathbf{A} = \mathbf{U}\mathbf{\Lambda}\mathbf{U}^T$, the bias of PnP is greater than the bias of graph Laplacian, i.e.,

$$\text{Bias}_L^i \leq \text{Bias}_P^i \quad (35)$$

if and only if the parameters $(\alpha_i, s_i, \lambda, \rho)$ satisfy the condition

$$\begin{aligned} (\rho - \lambda s_i) \left[-2\alpha_i^3(1 - \alpha_i)s_i + 2\lambda\rho(1 - s_i)^2 + \dots \right. \\ \left. + \alpha_i(2\alpha_i - 1)(1 - s_i)(\rho + \lambda s_i) \right] \leq 0. \end{aligned} \quad (36)$$

Before we prove the result, it will be useful to look at a special case where we can have a more ‘‘civilized’’ version of (36). Consider a denoising problem where $\mathbf{A} = \mathbf{I}$ and hence $\alpha_i = 1$ for all i . Then, (36) simplifies to

$$(\rho - \lambda s_i)[(\lambda - 2\lambda\rho)s_i + \rho + 2\lambda\rho] \leq 0,$$

which holds if the two terms in the product hold different signs. This gives us two cases:

- (i) $\rho - \lambda s_i \geq 0$, and $(\lambda - 2\lambda\rho)s_i + \rho + 2\lambda\rho \leq 0$,
- (ii) $\rho - \lambda s_i \leq 0$, and $(\lambda - 2\lambda\rho)s_i + \rho + 2\lambda\rho \geq 0$.

For case (i), if $\rho > \frac{1}{2}$, we have $s_i \leq \rho/\lambda$ and $s_i \geq \frac{\rho}{\lambda} \left(\frac{2\lambda+1}{2\rho-1} \right) \geq \frac{\rho}{\lambda}$ which is a contradiction except $s_i = \rho/\lambda$.

If $\rho < \frac{1}{2}$, we have $s_i \leq \rho/\lambda$ and $s_i \geq -\frac{\rho}{\lambda} \left(\frac{2\lambda+1}{1-2\rho} \right)$ which can be simplified to $s_i \leq \rho/\lambda$ since $s_i \geq 0$. Similar arguments hold for case (ii), and we can conclude that

$$s_i \leq \frac{\rho}{\lambda} \text{ if } \rho < \frac{1}{2} \text{ or } s_i \geq \frac{\rho}{\lambda} \text{ if } \rho \geq \frac{1}{2}. \quad (37)$$

In practice ρ is typically much smaller than $1/2$. Thus, if $\mathbf{A} = \mathbf{I}$, then $\text{Bias}_L^i \leq \text{Bias}_P^i$ for any $s_i \geq \rho/\lambda$ with $\rho < 1/2$.

Proof. For notational simplicity we drop the subscript i . To show $\text{Bias}_L^i - \text{Bias}_P^i \leq 0$, we cross multiply the numerators and denominators. Since the denominators are positive, it remains to check the combined numerator, which leads us to show

$$\begin{aligned} (\alpha^2 + \lambda - \lambda s - \alpha)^2 (\alpha^2 s - \rho s + \rho)^2 \\ - (\alpha^2 s - \rho s + \rho - \alpha s)^2 (\alpha^2 + \lambda - \lambda s)^2 \leq 0. \end{aligned}$$

Since the left hand side is a difference of two square terms, the expression can be simplified to

$$\begin{aligned} \left[\alpha(1-s)(\rho - \lambda s) \right] \left[-2\alpha^3(1-\alpha)s + \dots \right. \\ \left. + \alpha(2\alpha - 1)(1-s)(\rho + \lambda s) + 2\lambda\rho(1-s)^2 \right] \leq 0. \end{aligned}$$

In addition, since $0 \leq \alpha \leq 1$, $0 \leq s \leq 1$, $\lambda > 0$ and $\rho > 0$, the term $\alpha(1-s)$ is always positive. Therefore, $\text{Bias}_L^i \geq \text{Bias}_P^i$ if and only if the product of the rest is positive. \square

The analysis of the variance can be carried out in a similar way. The variance of the estimates are

$$\text{Var}_L^i = \frac{\sigma_\eta^2 \alpha_i^2}{(\alpha_i^2 + \lambda - \lambda s_i)^2}, \quad \text{and} \quad \text{Var}_P^i = \frac{\sigma_\eta^2 \alpha_i^2 s_i^2}{(\alpha_i^2 s_i - \rho s_i + \rho)^2}.$$

Proposition 2. Assume $\mathbf{A} = \mathbf{U}\mathbf{\Lambda}\mathbf{U}^T$, the variance of PnP is less than the variance of graph Laplacian, i.e.,

$$\text{Var}_L^i \geq \text{Var}_P^i, \quad (38)$$

if and only if $s_i \leq \frac{\rho}{\lambda}$.

Proof. For notational simplicity we drop the subscript i . To show $\text{Var}_L^i - \text{Var}_P^i \geq 0$, we show that

$$\begin{aligned} & (\alpha^2 s - \rho s + \rho)^2 - s^2(\alpha^2 + \lambda - \lambda s)^2 \\ &= [2\alpha^2 s + (1-s)(\rho + \lambda s)] [(1-s)(\rho - \lambda s)] \geq 0 \end{aligned}$$

if and only if $\rho - \lambda s \geq 0$, because the rest of the terms are all positive. \square

Unlike the bias result in (36) which depends on the spectrum of \mathbf{A} , the variance result in (38) holds for any \mathbf{A} . Now, if we restrict ourselves to $\mathbf{A} = \mathbf{I}$, then we can show a *phase transition point* ρ/λ such that for any $s_i \leq \rho/\lambda$ the variance is lower and for any $s_i \geq \rho/\lambda$ the bias is lower. Since s_i is a decreasing function of i , it implies that there exists i^* such that for any $i \geq i^*$ we have $s_i \leq \rho/\lambda$ and for any $i \leq i^*$ we have $s_i \geq \rho/\lambda$. In other words, we can quantify the bias and variance as follows.

Proposition 3. Assume $\mathbf{A} = \mathbf{I}$ and $\rho < 1/2$. There exists a phase transition point i^* such that

$$\begin{aligned} \text{Var}_L^i &\geq \text{Var}_P^i, \quad \forall i \geq i^*, \\ \text{Bias}_L^i &\leq \text{Bias}_P^i, \quad \forall i \leq i^*. \end{aligned} \quad (39)$$

The index i^* corresponds to the nearest integer i such that $s_i = \rho/\lambda$.

To numerically verifying the findings, we conduct the same experiment as in Figure 2 but with $\mathbf{A} = \mathbf{I}$. (Here we set $\rho = 0.1$ and $\lambda = 0.9$ to match a typical value of ρ and λ .) The results are shown in Figure 3, where we make two sets of plots. On the left hand side, we plot the MSE, the bias, and the variance as a function of the eigen-index i . As i increases, there is a clear transition at about $i^* = 140$ such that for any $i \geq i^*$ the variance of PnP is lower, and for any $i \leq i^*$ the bias of PnP is lower. On the right hand side of Figure 3, we plot the eigenvalue s_i as a function of i and we overlay the line ρ/λ (which is approximately 0.1 in this experiment). The cut off is exactly specified by $i^* = 140$. The bottom right plots of Figure 3 shows the bias and variance as a function of s_i . If $s_i \leq \rho/\lambda$, the bottom plots show that the variance of PnP is lower. If $s_i \geq \rho/\lambda$, the bottom plots show that the bias of PnP is lower.

E. Sensitivity of \mathbf{W}

The performance of PnP is heavily influenced by how well \mathbf{W} is estimated. If \mathbf{W} is estimated from the noisy input \mathbf{y} , the performance of PnP will degrade. We conduct an experiment to understand the degradation by constructing a pre-filtered signal via $\hat{\mathbf{x}}_{\text{pre}} = \mathbf{x} + \boldsymbol{\epsilon}$, where $\mathbf{x} \in \mathbb{R}^n$ is the true signal, and $\boldsymbol{\epsilon} \sim \mathcal{N}(\mathbf{0}, \sigma_\epsilon^2 \mathbf{I})$. The graph filter is constructed \mathbf{W} using $\hat{\mathbf{x}}_{\text{pre}}$,

where the kernel matrix \mathbf{K} is a non-local mean filter used in Figure 2. The constructed \mathbf{W} is now a function of $\hat{\mathbf{x}}_{\text{pre}}$.¹

When \mathbf{W} is estimated from $\hat{\mathbf{x}}_{\text{pre}}$, the energy concentration capability of \mathbf{W} drops. Figure 4 shows the eigenvalue s_i as a function i for $\sigma_\epsilon \in [0, 0.2]$. As we can see from the figure, if we fix $\rho = 0.1$ and $\lambda = 0.9$, the transition point i^* shifts to a large index when noise level σ_ϵ increases. Consequently, $\text{Var}_L^i \geq \text{Var}_P^i$ takes place for a narrower range of i 's, whereas $\text{Bias}_L^i \leq \text{Bias}_P^i$ happens for a wider range of i 's. Since the variance usually has a bigger margin than the bias when we compare PnP with graph Laplacian (See Figure 3), MSE will become worse as we increase σ_ϵ .

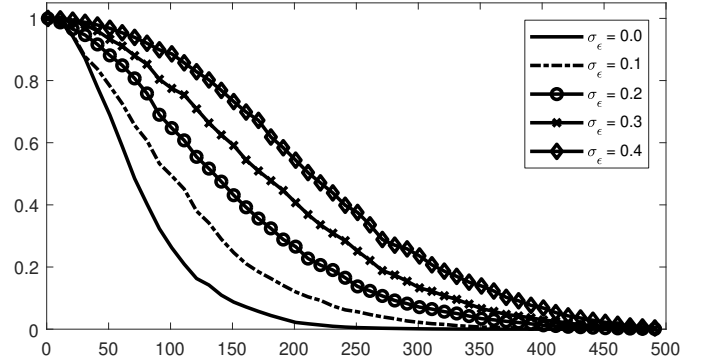


Fig. 4. Energy concentration of $\mathbf{W}(\hat{\mathbf{x}}_{\text{pre}})$ as σ_ϵ increases. The plot shows the eigenvalue s_i of \mathbf{W} as a function of the eigen-index i . As σ_ϵ increases, the decay rate of s_i reduces and so for the cutoff index i^* shifts towards the right.

Figure 5 shows another plot of the same experiment, where we compute the MSE by running PnP on a deblurring problem using the \mathbf{A} and \mathbf{W} defined in Figure 2. We set $\rho = 0.1$ and $\lambda = 0.9$. We observe that PnP has a considerably lower MSE than graph Laplacian when σ_ϵ is small. However, as σ_ϵ increases, MSE_P quickly increases and eventually goes above MSE_L . This shows that while PnP has better performance than graph Laplacian, it is also more sensitive to any error in \mathbf{W} compared to graph Laplacian.

F. Geometric Interpretation

A qualitative interpretation of the result can be seen by revisiting g defined in (17). For any forward model $f(\mathbf{x})$, the optimization solved by PnP is

$$\begin{aligned} \hat{\mathbf{x}}_P &= \underset{\mathbf{x}}{\text{argmin}} \quad f(\mathbf{x}) + \frac{\rho}{2} \mathbf{x}^T \mathbf{U}_1 (\mathbf{S}_1^{-1} - \mathbf{I}) \mathbf{U}_1^T \mathbf{x} \\ &\text{subject to} \quad \mathbf{U}_2^T \mathbf{x} = \mathbf{0}. \end{aligned} \quad (40)$$

The optimization solved by graph Laplacian is

$$\begin{aligned} \hat{\mathbf{x}}_L &= \underset{\mathbf{x}}{\text{argmin}} \quad f(\mathbf{x}) + \frac{\lambda}{2} \mathbf{x}^T \mathbf{U}_1 (\mathbf{I} - \mathbf{S}_1) \mathbf{U}_1^T \mathbf{x} \\ &\quad + \frac{\lambda}{2} \mathbf{x}^T \mathbf{U}_2 (\mathbf{I} - \mathbf{S}_2) \mathbf{U}_2^T \mathbf{x}, \end{aligned}$$

¹An alternative experiment would be to pick a specific baseline denoising algorithm and adjust its internal parameters. However, different baseline denoising algorithms have different characteristics and this could cause bias in the analysis. Thus, we choose to design a pre-filtered signal by adding iid noise.

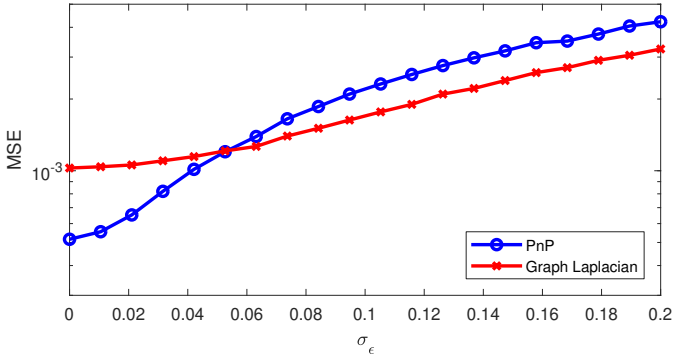


Fig. 5. Influence of the pre-filtered signal quality to MSE. The experiment uses the \mathbf{A} and \mathbf{W} as in Figure 2. The parameter σ_ϵ determines the amount of perturbation in $\hat{\mathbf{x}}_{\text{pre}}$.

which, if we let $\mathbf{S}_2 = \mathbf{0}$, is simplified to

$$\hat{\mathbf{x}}_L = \underset{\mathbf{x}}{\operatorname{argmin}} f(\mathbf{x}) + \frac{\lambda}{2} \left(\mathbf{x}^T \mathbf{U}_1 (\mathbf{I} - \mathbf{S}_1) \mathbf{U}_1^T \mathbf{x} + \|\mathbf{U}_2^T \mathbf{x}\|^2 \right). \quad (41)$$

The constraint in (40) provides a strong restriction on \mathbf{x} . Rather than searching through the entire column space of \mathbf{W} , PnP ADMM only searches for a subspace spanned by eigenvectors \mathbf{U}_1 . Because of the energy concentration property of \mathbf{W} , any \mathbf{x} living in the null space $\mathbf{U}_2^T \mathbf{x} = \mathbf{0}$ will correspond to noise and no signal. Therefore, by restricting $\mathbf{U}_2^T \mathbf{x} = \mathbf{0}$ we essentially eliminate the pure noise component observed in \mathbf{y} . This is useful, because it suggests that before we even solve the minimization (40), a large portion of the noise is already cleaned by forcing $\mathbf{U}_2^T \mathbf{x} = \mathbf{0}$. Figure 6 illustrates the concept pictorially. In graph Laplacian (41), the hard constraint $\mathbf{U}_2^T \mathbf{x} = \mathbf{0}$ becomes a regularization term $\|\mathbf{U}_2^T \mathbf{x}\|^2$. However, since $\|\mathbf{U}_2^T \mathbf{x}\|^2$ share the same λ with $\mathbf{x}^T \mathbf{U}_1 (\mathbf{I} - \mathbf{S}_1) \mathbf{U}_1^T \mathbf{x}$, it can never reach $\|\mathbf{U}_2^T \mathbf{x}\|^2 = 0$.

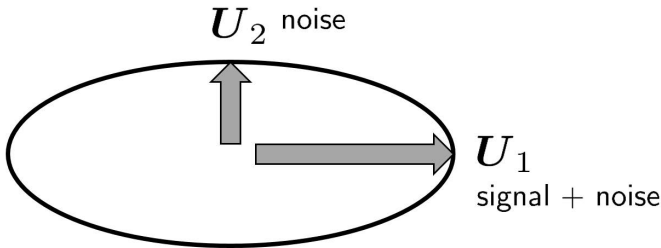


Fig. 6. PnP ADMM decomposes the optimization variable \mathbf{x} into two subspaces \mathbf{U}_1 and \mathbf{U}_2 . By restricting \mathbf{x} such that $\mathbf{U}_2^T \mathbf{x} = \mathbf{0}$, we eliminate the noise living in \mathbf{U}_2 .

Does a better denoiser give a better PnP ADMM algorithm? The exact answer is unclear because modern denoisers are nonlinear. However, if we focus on linear denoisers, then our analysis suggests that the performance is caused by the rejection of noise before solving the inverse problem. In the extreme case when \mathbf{W} contains only one non-zero eigenvalue which corresponds to the oracle eigenvector $\mathbf{x}/\|\mathbf{x}\|_2$, \mathbf{U}_2 will consist of $n - 1$ columns that are orthogonal to $\mathbf{x}/\|\mathbf{x}\|_2$. By restricting $\mathbf{U}_2^T \mathbf{x} = \mathbf{0}$, we are guaranteed to recover \mathbf{x} exactly. On the other extreme, if \mathbf{W} is a random matrix or a matrix that does not separate noise from the signal, then the

energy concentration property will fail and hence the constraint $\mathbf{U}_2^T \mathbf{x} = \mathbf{0}$ will have zero or even negative influence.

IV. PERFORMANCE ANALYSIS VIA EQUILIBRIUM

The MAP optimization in (1) is not the only way to obtain $\hat{\mathbf{x}}$. In [22], Buzzard *et al.* generalize PnP ADMM by analyzing the equilibrium state of a dynamical system. In this section we approach the problem from such equilibrium perspective.

A. Consensus Equilibrium

To understand the concept of consensus equilibrium, we start by defining a pair of functions F and G using (4) and (5) respectively. We can show that at convergence, the PnP ADMM solution $(\hat{\mathbf{x}}, \hat{\mathbf{u}})$ satisfies

$$\hat{\mathbf{x}} = F(\hat{\mathbf{x}} + \hat{\mathbf{u}}), \quad (42)$$

$$\hat{\mathbf{x}} = G(\hat{\mathbf{x}} - \hat{\mathbf{u}}). \quad (43)$$

We call such solution $(\hat{\mathbf{x}}, \hat{\mathbf{u}})$ the consensus equilibrium of (42)-(43). The following proposition defines the consensus equilibrium of PnP for a linear inverse problem.

Proposition 4. Consider two operators F and G :

$$F(\mathbf{x}) = \underset{\mathbf{v} \in \mathbb{R}^n}{\operatorname{argmin}} \frac{1}{2} \|\mathbf{A}\mathbf{v} - \mathbf{y}\|^2 + \frac{\rho}{2} \|\mathbf{v} - \mathbf{x}\|^2,$$

$$G(\mathbf{x}) = \mathbf{W}\mathbf{x}$$

The consensus equilibrium $(\hat{\mathbf{x}}, \hat{\mathbf{u}})$ satisfies

$$\left(\mathbf{W}(\mathbf{A}^T \mathbf{A} - \rho \mathbf{I}) + \rho \mathbf{I} \right) \hat{\mathbf{x}} = \mathbf{W} \mathbf{A}^T \mathbf{y}, \quad (44a)$$

$$\mathbf{W} \hat{\mathbf{u}} = (\mathbf{W} - \mathbf{I}) \hat{\mathbf{x}}. \quad (44b)$$

Proof. Since $G(\mathbf{x}) = \mathbf{W}\mathbf{x}$, it holds that $G(\hat{\mathbf{x}} - \hat{\mathbf{u}}) = \mathbf{W}(\hat{\mathbf{x}} - \hat{\mathbf{u}})$, which implies that $\mathbf{W}\hat{\mathbf{u}} = \mathbf{W}\hat{\mathbf{x}} - \hat{\mathbf{x}}$. The optimality of F gives

$$(\mathbf{A}^T \mathbf{A} + \rho \mathbf{I}) \hat{\mathbf{x}} = \mathbf{A}^T \mathbf{y} + \rho(\hat{\mathbf{x}} + \hat{\mathbf{u}}).$$

Multiplying both sides by \mathbf{W} yields

$$\mathbf{W}(\mathbf{A}^T \mathbf{A} + \rho \mathbf{I}) \hat{\mathbf{x}} = \mathbf{W} \mathbf{A}^T \mathbf{y} + \rho \mathbf{W}(\hat{\mathbf{x}} + \hat{\mathbf{u}}).$$

Substituting $\mathbf{W}\hat{\mathbf{u}} = \mathbf{W}\hat{\mathbf{x}} - \hat{\mathbf{x}}$, and rearranging the terms we can show the desired result. \square

Proposition 4 is useful in the sense that for a given solution $\hat{\mathbf{x}}$, we can easily check whether it is a consensus equilibrium point without going through the PnP ADMM algorithm. This allows us to “create” alternative optimization formulations and see if the solution is the desired equilibrium point. To illustrate this idea, let us consider two examples.

Example 1. When $\mathbf{A} = \mathbf{I}$. This is a denoising problem where $f(\mathbf{x}) = \frac{1}{2} \|\mathbf{x} - \mathbf{y}\|^2$. The proposition below shows three optimizations that have the same equilibrium.

Proposition 5. Define the functions φ , ψ_1 and ψ_2 :

$$\varphi(\mathbf{x}) = \frac{1}{2} \|\mathbf{x} - \mathbf{y}\|^2 + \lambda g(\mathbf{x}), \quad (45)$$

$$\psi_1(\mathbf{x}) = \frac{1}{2} \|\mathbf{x} - \mathbf{W}\mathbf{y}\|^2 - \frac{(1-\rho)}{2} \mathbf{x}^T (\mathbf{I} - \mathbf{W}) \mathbf{x}, \quad (46)$$

$$\psi_2(\mathbf{x}) = \frac{1}{2} \left\| \mathbf{x} - [(1-\rho)\mathbf{W} + \rho\mathbf{I}]^{-1} \mathbf{W}\mathbf{y} \right\|^2, \quad (47)$$

where $g(\mathbf{x})$ is defined in (17). Then, the minimizers of these functions all satisfy the equilibrium condition (44a)-(44b).

Proof. To prove ψ_1 , we substitute $\mathbf{A} = \mathbf{I}$ into the matrix in (44a), and show that $\mathbf{W}(\mathbf{I} - \rho\mathbf{I}) + \rho\mathbf{I} = \mathbf{I} - (1 - \rho)(\mathbf{I} - \mathbf{W})$. Therefore, the equilibrium condition becomes $\mathbf{x} = [\mathbf{I} - (1 - \rho)(\mathbf{I} - \mathbf{W})]^{-1} \mathbf{W}\mathbf{y}$, which is equivalent to the first order optimality of (46). ψ_2 is just a restatement of the equilibrium, put in an optimization form. \square

In Proposition 5, the first optimization of φ is the MAP formulation we saw in Section 3. The third optimization ψ_2 , is very different from φ but it has the same equilibrium as φ . (Of course, one can argue that ψ_2 is useless because it is just a re-statement of the solution.)

The optimization of ψ_1 is interesting in the sense that it is different from φ , but it still resembles the same equilibrium. The objective function $\frac{1}{2}\|\mathbf{x} - \mathbf{W}\mathbf{y}\|^2$ says that instead of trying to minimize the residue between the optimization variable \mathbf{x} and the noisy observation \mathbf{y} , we minimize \mathbf{x} with the filtered version $\mathbf{W}\mathbf{y}$. For oracle \mathbf{W} 's where pure noise components are isolated at high frequencies, $\mathbf{W}\mathbf{y}$ ensures that the pure noise components are eliminated. Therefore, when minimizing $\frac{1}{2}\|\mathbf{x} - \mathbf{W}\mathbf{y}\|^2$, we are guaranteed to only search for the signal component.

The regularization term $-\frac{(1-\rho)}{2}\mathbf{x}^T(\mathbf{I} - \mathbf{W})\mathbf{x}$ is a concave function for any $0 \leq \rho \leq 1$, because $\mathbf{I} - \mathbf{W}$ is positive semi-definite. The concave function *injects* high frequency components that are lost by $\mathbf{W}\mathbf{y}$. In the extreme cases when $\rho = 1$, we have

$$\psi_1(\mathbf{x}) = \frac{1}{2}\|\mathbf{x} - \mathbf{W}\mathbf{y}\|^2,$$

and so the minimizer is just $\hat{\mathbf{x}} = \mathbf{W}\mathbf{y}$. When $\rho = 0$, we have

$$\psi_1(\mathbf{x}) = \frac{1}{2}\|\mathbf{x} - \mathbf{W}\mathbf{y}\|^2 - \frac{1}{2}\mathbf{x}^T(\mathbf{I} - \mathbf{W})\mathbf{x}.$$

By expanding the terms we can show that

$$\begin{aligned} \psi_1(\mathbf{x}) &= \frac{1}{2}\|\mathbf{x}\|^2 - \mathbf{x}^T\mathbf{W}\mathbf{y} + \frac{1}{2}\|\mathbf{W}\mathbf{y}\|^2 - \frac{1}{2}\|\mathbf{x}\|^2 + \frac{1}{2}\mathbf{x}^T\mathbf{W}\mathbf{x} \\ &= \frac{1}{2}(\mathbf{x} - \mathbf{y})^T\mathbf{W}(\mathbf{x} - \mathbf{y}) + \frac{1}{2}\mathbf{y}^T\mathbf{W}(\mathbf{W} - \mathbf{I})\mathbf{y}, \end{aligned}$$

and so the minimizer is $\hat{\mathbf{x}} = \mathbf{y}$. In order to control the amount of high frequency injection, a small ρ is more preferred than a large ρ . This explains why in Figure 2 a smaller ρ works better for PnP ADMM.

Example 2. When $\mathbf{A} = \mathbf{U}\mathbf{\Lambda}\mathbf{U}^T$. In this example, we consider an inverse problem $f(\mathbf{x}) = \frac{1}{2}\|\mathbf{A}\mathbf{x} - \mathbf{y}\|^2$ for $\mathbf{A} = \mathbf{U}\mathbf{\Lambda}\mathbf{U}^T$, where \mathbf{U} is the eigenvector of \mathbf{W} . The proposition below shows two equivalent formulations.

Proposition 6. Let $\mathbf{A} = \mathbf{U}\mathbf{\Lambda}\mathbf{U}^T$, where \mathbf{U} is the eigenvector of \mathbf{W} . Define two functions φ and ψ

$$\varphi(\mathbf{x}) = \frac{1}{2}\|\mathbf{A}\mathbf{x} - \mathbf{y}\|^2 + \lambda g(\mathbf{x}), \quad (48)$$

$$\psi(\mathbf{x}) = \frac{1}{2}(\mathbf{A}\mathbf{x} - \mathbf{y})^T\mathbf{W}(\mathbf{A}\mathbf{x} - \mathbf{y}) + \frac{\rho}{2}\mathbf{x}^T(\mathbf{I} - \mathbf{W})\mathbf{x}, \quad (49)$$

where $g(\mathbf{x})$ is defined in (17). Then, the minimizers of these functions all satisfy the equilibrium condition (44a)-(44b).

Proof. Since $\mathbf{A} = \mathbf{U}\mathbf{\Lambda}\mathbf{U}^T$ and $\mathbf{W} = \mathbf{U}\mathbf{S}\mathbf{U}^T$, it holds that \mathbf{A} commutes with \mathbf{W} , i.e., $\mathbf{W}\mathbf{A} = \mathbf{A}\mathbf{W}$. Thus, the consensus condition can be written as

$$\left[\mathbf{A}^T\mathbf{W}\mathbf{A} + \rho(\mathbf{I} - \mathbf{W}) \right] \hat{\mathbf{x}} = \mathbf{A}^T\mathbf{W}\mathbf{y},$$

which is the first order optimality condition of the optimization

$$\underset{\mathbf{x}}{\text{minimize}} \quad \frac{1}{2} \left\| \mathbf{W}^{\frac{1}{2}}\mathbf{A}\mathbf{x} - \mathbf{W}^{\frac{1}{2}}\mathbf{y} \right\|^2 + \frac{\rho}{2}\mathbf{x}^T(\mathbf{I} - \mathbf{W})\mathbf{x}.$$

Expanding the first term yields the desired result. \square

The function ψ can be interpreted as follows. If \mathbf{W} contains zero eigenvalues, the objective $(\mathbf{A}\mathbf{x} - \mathbf{y})^T\mathbf{W}(\mathbf{A}\mathbf{x} - \mathbf{y})$ will have no cost along those eigenvectors. As a result, since the regularization $\mathbf{x}^T(\mathbf{I} - \mathbf{W})\mathbf{x}$ is minimized at $\mathbf{U}^T\mathbf{x} = \mathbf{0}$, we must have $\mathbf{U}_2^T\mathbf{x} = \mathbf{0}$ if those eigenvectors with zero eigenvalues.

Rewriting the optimization in terms of ψ also allows us to connect with other works in the literature. In [29], Kheradmand and Milanfar suggest minimizing the following cost when solving a linear inverse problem²:

$$\psi(\mathbf{x}) = \frac{1}{2} \|\mathbf{A}\mathbf{x} - \mathbf{y}\|_{\mathbf{P}}^2 + \frac{\rho}{2}\mathbf{x}^T(\mathbf{I} - \mathbf{W})\mathbf{x}, \quad (50)$$

where $\mathbf{P} = \mathbf{I} + \beta(\mathbf{I} - \mathbf{W})$ for some $\beta \geq -1$. This is more general formulation than ours, because if we let $\beta = -1$, then we obtain (49).

In summary, the two examples above show that if we are willing to change the forward model $f(\mathbf{x})$ by integrating the denoiser into $f(\mathbf{x})$, then there are more than optimization formulations which can offer meaningful interpretations while satisfying the equilibrium condition.

B. Performance of Multiple Priors

Beyond a single denoiser we can extend the equilibrium analysis for multiple denoisers. In this case, the MAP-based optimization is

$$\hat{\mathbf{x}} = \underset{\mathbf{x} \in \mathbb{R}^n}{\text{argmin}} \quad \varphi(\mathbf{x}) \stackrel{\text{def}}{=} \mu_0 f_0(\mathbf{x}) + \sum_{i=1}^k \mu_i f_i(\mathbf{x}), \quad (51)$$

where $f_0 : \mathbb{R}^n \rightarrow \mathbb{R}$ is objective function associated with the forward model, and $\{f_i\}_{i=1}^k$ are the regularization functions associated with the prior models (if they exist).

Putting into the equilibrium framework, the operations are

$$\begin{aligned} F_0(\mathbf{x}) &= \underset{\mathbf{z} \in \mathbb{R}^n}{\text{argmin}} \quad f_0(\mathbf{z}) + \frac{\rho}{2}\|\mathbf{z} - \mathbf{x}\|^2, \\ F_i(\mathbf{x}) &= \mathbf{W}_i\mathbf{x}, \quad i = 1, \dots, k. \end{aligned}$$

At equilibrium, the solution $(\hat{\mathbf{x}}, \{\hat{\mathbf{u}}_i\}_{i=0}^k)$ satisfies

$$F_i(\hat{\mathbf{x}} + \hat{\mathbf{u}}_i) = \hat{\mathbf{x}}, \quad \text{and} \quad \sum_{i=0}^k \mu_i \hat{\mathbf{u}}_i = \mathbf{0}, \quad (52)$$

which is a generalization of the case $k = 2$ in (42) and (43). In (52), The mappings $\{F_i\}_{i=0}^k$ are called *agents*, whose relative strengths are controlled by the parameters $\{\mu_i\}_{i=0}^k$.

²The work in [29] considers a general \mathbf{A} matrix and not only $\mathbf{A} = \mathbf{U}\mathbf{\Lambda}\mathbf{U}^T$.

Without loss of generality we assume that $\sum_{i=1}^k \mu_i = 1$, and μ_0 can take any positive value. The intuition behind (52) is the concept of assembling individual experts to produce an overall better result. For example, F_i could represent image denoisers trained by different image classes, e.g., human faces, buildings and plants, etc. Given an unknown scene, it is likely that one of the denoisers would perform better than the others. Therefore, an ensemble of weak experts can improve the robustness against model mismatch.

To make the following discussion more concrete, let us focus on the forward model $f_0(\mathbf{x}) = \frac{1}{2} \|\mathbf{A}\mathbf{x} - \mathbf{y}\|^2$ for an arbitrary \mathbf{A} (not necessarily $\mathbf{A} = \mathbf{U}\mathbf{\Lambda}\mathbf{U}^T$) but assume that \mathbf{W}_i is invertible. Then, the agent F_0 is defined as

$$\begin{aligned} F_0(\mathbf{x}) &= \underset{\mathbf{v}}{\operatorname{argmin}} \frac{1}{2} \|\mathbf{A}\mathbf{v} - \mathbf{y}\|^2 + \frac{\rho}{2} \|\mathbf{v} - \mathbf{x}\|^2 \\ &= (\mathbf{A}^T \mathbf{A} + \rho \mathbf{I})^{-1} (\mathbf{A}^T \mathbf{y} + \rho \mathbf{x}). \end{aligned}$$

The equilibrium condition can be determined by substituting $\mathbf{x} = \hat{\mathbf{x}} + \hat{\mathbf{u}}_0$, leading to

$$\hat{\mathbf{x}} = F_0(\hat{\mathbf{x}} + \hat{\mathbf{u}}_0) = (\mathbf{A}^T \mathbf{A} + \rho \mathbf{I})^{-1} (\mathbf{A}^T \mathbf{y} + \rho(\hat{\mathbf{x}} + \hat{\mathbf{u}}_0)).$$

Rearranging the terms gives $\hat{\mathbf{u}}_0 = \frac{1}{\rho} \mathbf{A}^T \mathbf{A} \hat{\mathbf{x}} - \frac{1}{\rho} \mathbf{A}^T \mathbf{y}$. For the remaining $k-1$ agents, we have

$$\hat{\mathbf{x}} = F_i(\hat{\mathbf{x}} + \hat{\mathbf{u}}_i) = \mathbf{W}_i(\hat{\mathbf{x}} + \hat{\mathbf{u}}_i) \Rightarrow \hat{\mathbf{u}}_i = (\mathbf{W}_i^{-1} - \mathbf{I})\hat{\mathbf{x}}.$$

Substituting into $\sum_{i=0}^k \mu_i \hat{\mathbf{u}}_i = \mathbf{0}$, we can show that the consensus equilibrium solution satisfies

$$\left(\frac{\mu_0}{\rho} \mathbf{A}^T \mathbf{A} + \sum_{i=1}^k \mu_i (\mathbf{W}_i^{-1} - \mathbf{I}) \right) \hat{\mathbf{x}} = \frac{\mu_0}{\rho} \mathbf{A}^T \mathbf{y}, \quad (53)$$

for $i = 1, \dots, k$.

To visually see the benefit of the combination, we consider a simple experiment where \mathbf{A} is the blur matrix used in Figure 2. We use $k = 5$ filters $\{\mathbf{W}_i\}_{i=1}^k$ where the filters \mathbf{W}_i are generated from kernels with different denoising strengths, see (9). The combination weights are set as $\mu_i = 1/k$ for simplicity, and we set $\mu_0 = 1$ and $\rho = 0.005$. The equilibrium condition of this combined filter gives a solution of the form

$$\hat{\mathbf{x}} = \left(\mu_0 \mathbf{A}^T \mathbf{A} + \rho \left(\sum_{i=1}^k \mu_i \mathbf{W}_i^{-1} - \mathbf{I} \right) \right)^{-1} \mu_0 \mathbf{A}^T \mathbf{y}. \quad (54)$$

For comparison, we also consider solutions obtained from a single filter. This leads to a solution

$$\hat{\mathbf{x}}_i = \left(\mu_0 \mathbf{A}^T \mathbf{A} + \rho (\mathbf{W}_i^{-1} - \mathbf{I}) \right)^{-1} \mu_0 \mathbf{A}^T \mathbf{y}, \quad (55)$$

for $i = 1, \dots, k$. Figure 7 shows the eigenvalue of the respective inversion matrices. The legend \mathbf{W}_i in the plot denotes the individual filters we use, and the legend \mathbf{W} denotes the combined filter. PSNR values of each method is shown in the legend. As one can see, the combined estimate staying in the middle \mathbf{W}_3 and \mathbf{W}_4 , which are the two best performing matrices.

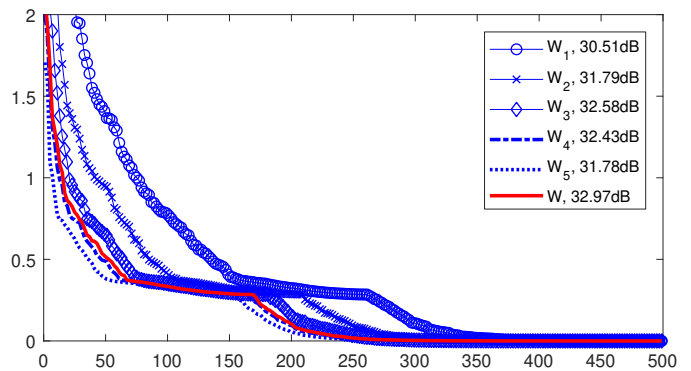


Fig. 7. Combining multiple priors for a deblurring problem. The curves show the eigenvalues of the inversion matrices defined in (54) and (55). We set $\rho = 0.005$, $\mu_0 = 1$, $\mu_i = 0.2$ for $i = 1, \dots, 5$.

C. Choosing the Weights

Is it possible to determine a set of weights $\{\mu_i\}_{i=1}^k$ so that they are optimal in some sense? In principle this is doable by minimizing the mean squared error between the $\hat{\mathbf{x}}$ defined in (54) and the ground truth (if we have access to). However, such approach is computationally prohibited because the $\{\mu_i\}_{i=1}^k$ are located in the denominator of (54).

A slightly more ad hoc approach is to solve (55) for every $\hat{\mathbf{x}}_i$, and define $\hat{\mathbf{x}}$ as a linear combination of them:

$$\hat{\mathbf{x}} = \sum_{i=1}^k \mu_i \hat{\mathbf{x}}_i = \sum_{i=1}^k \mu_i \mathbf{Q}_i^{-1} \mathbf{A}^T \mathbf{y}, \quad (56)$$

where $\mathbf{Q}_i \stackrel{\text{def}}{=} \left(\mathbf{A}^T \mathbf{A} + (\rho/\mu_i)(\mathbf{W}_i^{-1} - \mathbf{I}) \right)$. An interpretation of (56) is the solution of an optimization

$$\min_{\hat{\mathbf{x}}, \{\mu_i\}_{i=1}^k} \sum_{i=1}^k \mu_i \|\hat{\mathbf{x}} - \hat{\mathbf{x}}_i\|^2 \quad (57)$$

$$\text{subject to } \left(\frac{\mu_0}{\rho} \mathbf{A}^T \mathbf{A} + (\mathbf{W}_i^{-1} - \mathbf{I}) \right) \hat{\mathbf{x}}_i = \frac{\mu_0}{\rho} \mathbf{A}^T \mathbf{y},$$

which says that among the individual equilibrium solutions $\hat{\mathbf{x}}_i$, we are finding an average $\hat{\mathbf{x}}$ that is close to all $\hat{\mathbf{x}}_i$'s.

The weighted average in (56) provides a simple way of determining $\{\mu_i\}_{i=1}^k$. Assuming that we have access to the ground truth \mathbf{x} , the weights $\{\mu_i\}_{i=1}^k$ can be found by minimizing

$$\min_{\{\mu_i\}_{i=1}^k} \left\| \mathbf{x} - \sum_{i=1}^k \mu_i \hat{\mathbf{x}}_i \right\|^2 \quad \text{subject to } \sum_{i=1}^k \mu_i = 1. \quad (58)$$

Letting $\boldsymbol{\mu} = [\mu_1, \dots, \mu_k]^T$, and defining the matrix $\boldsymbol{\Sigma} \in \mathbb{R}^{k \times k}$ such that $[\boldsymbol{\Sigma}]_{ij} = (\mathbf{x} - \hat{\mathbf{x}}_i)^T (\mathbf{x} - \hat{\mathbf{x}}_j)$, then (58) can be written as

$$\min_{\boldsymbol{\mu}} \boldsymbol{\mu}^T \boldsymbol{\Sigma} \boldsymbol{\mu} \quad \text{subject to } \boldsymbol{\mu}^T \mathbf{1} = 1. \quad (59)$$

Closed-form solution of (59) exists, and is given by

$$\boldsymbol{\mu}^* = \frac{\boldsymbol{\Sigma}^{-1} \mathbf{1}}{\mathbf{1}^T \boldsymbol{\Sigma}^{-1} \mathbf{1}}. \quad (60)$$

Readers interested in the details can refer to [42] by Choi *et al.*, where they discuss the solution's geometry and its extension to cases where ground truth is not available.

TABLE I

INPAINTING EXPERIMENT. THE INPUT IMAGES CONTAINS OF UNIFORMLY RANDOM SAMPLED PIXELS AT A RATE OF 80%, 60%, 40%, AND 20%. THE RECONSTRUCTION METHODS ARE GRAPH LAPLACIAN (LPS) AND PnP ADMM (PnP). THE REGULARIZATION PARAMETER ρ AND λ ARE OPTIMIZED FOR EVERY IMAGE AND EVERY CONFIGURATION.

Img	Estimated \mathbf{W}								Oracle \mathbf{W}							
	80%		60%		40%		20%		80%		60%		40%		20%	
	Lps	PnP	Lps	PnP	Lps	PnP	Lps	PnP	Lps	PnP	Lps	PnP	Lps	PnP	Lps	PnP
Barb	26.86	28.97	26.30	27.88	25.75	26.80	23.64	24.36	50.47	53.50	48.72	52.41	47.14	50.58	44.26	49.11
Boat	26.64	28.54	25.93	27.31	25.16	25.96	23.04	23.46	50.16	51.92	48.84	51.89	47.10	50.01	43.64	48.01
Cmra	26.39	27.88	25.30	26.33	24.13	24.81	22.01	22.26	49.67	50.53	48.32	50.20	46.99	47.92	44.28	45.62
Coup	26.55	28.46	25.87	27.25	25.19	25.98	23.22	23.67	50.25	52.72	48.18	50.81	46.98	50.79	43.96	48.51
Hous	27.28	30.52	27.22	29.83	26.95	28.67	25.07	25.82	50.66	53.56	49.16	53.39	46.81	50.72	43.63	48.52
Lena	26.98	29.77	26.62	28.70	26.25	27.57	24.28	24.94	49.62	53.13	48.29	52.18	47.45	51.44	43.93	48.15
Man	26.81	29.10	26.39	28.12	25.80	26.85	23.95	24.58	50.19	53.27	49.05	52.06	47.23	51.17	44.08	49.25
Pepp	26.36	28.41	25.64	27.10	24.67	25.51	22.66	23.21	49.69	51.12	49.20	51.26	46.61	50.64	41.98	46.77

V. FURTHER DISCUSSIONS

We close the paper by discussing a few issues that might be of interest to readers.

• **Experiment on Images.** Thus far the numerical results are all based on 1D signals. Readers who do image processing may wonder how well can the theory be translated to images. To articulate this problem, we consider an inpainting problem which has a forward model as

$$\mathbf{y} = \mathbf{A}\mathbf{x} + \boldsymbol{\eta}. \quad (61)$$

In this equation, $\mathbf{A} \in \mathbb{R}^{m \times n}$ is a sampling matrix which either selects or not selects a pixel from the input image \mathbf{x} . The noise vector $\boldsymbol{\eta}$ is assumed i.i.d. Gaussian with standard deviation $\sigma_{\eta} = 0.05$. Therefore, the objective function is $f(\mathbf{x}) = \frac{1}{2} \|\mathbf{A}\mathbf{x} - \mathbf{y}\|^2$.

The result of this experiment is shown in Table I, where we compare graph Laplacian with PnP at different sampling ratios (20%, 40%, 60%, 80%). The \mathbf{W} matrix is generated from a non-local means kernel using a MATLAB code implementing the Nystrom method in [30]. The prefiltered signal is generated by using the Sheperd interpolation algorithm [43]. We test 8 “standard” images and report the PSNR. The regularization parameters ρ (or λ) are optimized for every image and for every testing condition. Therefore, the PSNRs shown in Table I are the best possible results of the methods. For both oracle and estimated \mathbf{W} , PnP ADMM is consistently better than graph Laplacian, which is coherent to the theoretical arguments.

• **Complexity Consideration.** When we compare (24) and (26), we tend to think that (24) is computationally less intensive because it is a standard least squares which can be solved using conjugate gradient (or other linear solvers). The PnP solution (26), on the other hand, requires spectral decomposition of \mathbf{W} so that we can obtain the solution via, e.g., by solving an optimization (40). However, a complexity analysis based on this line of argument is not totally correct because in order to obtain the PnP solution we actually use the ADMM algorithm (4)-(6). Thus, the real complexity bottleneck is at the inversion, i.e., (4), not the graph filter \mathbf{W} . For specific problems such as deblurring where $f(\mathbf{x})$ has structures, e.g., toeplitz matrix, the inversion could be done in $\mathcal{O}(n \log n)$ via Fourier transform.

• **Statistical Interpretations of \mathbf{W} and \mathbf{W}^{-1} .** If we regard \mathbf{W} as some kind of covariance matrix, then the inverse \mathbf{W}^{-1} is the precision matrix. The (i, j) -th element of the covariance matrix measures the *correlation* between node i and node j of the graph, whereas the (i, j) -th element of the precision matrix measures the *partial correlation* between node i and node j condition on all the other $n - 2$ nodes. Partial correlation is useful in handling situations where a high correlation between i and j is caused by some some third party node k . Thus by conditioning on k we can remove the dependency of node k , and leaving just the partial correlation between i and j .

As an example, in Figure 8 we show a ground truth signal \mathbf{x} used to generate a filter matrix \mathbf{W} . We then compute the pseudo-inverse \mathbf{W}^+ by keeping on the 50 leading eigenvectors, and plot its magnitude in the log-scale. (Note: We cannot compute the actual inverse \mathbf{W}^{-1} when \mathbf{W} is not invertible.) As we can see, while \mathbf{W} shows a banded diagonal behavior due to a spatial constraint we put, the inverse matrix \mathbf{W}^+ shows a very strong signal dependent behavior.

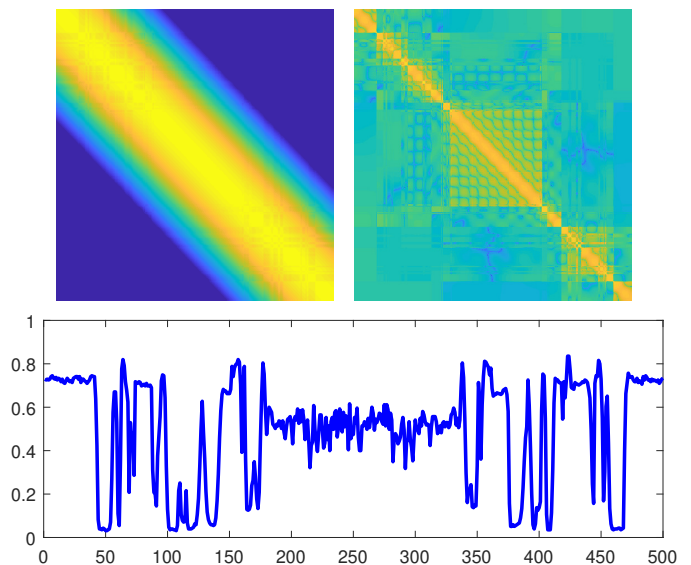


Fig. 8. [Top Left] \mathbf{W} . [Top Right] \mathbf{W}^+ , the pseudo-inverse of \mathbf{W} . We plot \mathbf{W} and \mathbf{W}^+ in log absolute scale so that we can visualize them. [Bottom] The ground truth signal \mathbf{x} used to generate \mathbf{W} .

• **Connection to RED.** A very similar idea to PnP ADMM is the regularization by denoising (RED) [17]. In RED, the idea

is to define the regularization by

$$g(\mathbf{x}) = \frac{1}{2} \mathbf{x}^T (\mathbf{x} - \mathcal{D}_\sigma(\mathbf{x})). \quad (62)$$

One advantage of such formulation is that we are able to interpret the regularization as the denoiser \mathcal{D}_σ is explicitly expressed in g . However, as recently discussed by Reehorst and Schniter [16], while RED offers an interpretable regularization, the existence of g is problematic if \mathcal{D}_σ is not symmetric.

If we restrict \mathcal{D}_σ to symmetric smoothing filters so that $\mathcal{D}_\sigma(\mathbf{x}) = \mathbf{W}\mathbf{x}$, then the RED regularization is nothing but

$$g(\mathbf{x}) = \frac{1}{2} \mathbf{x}^T (\mathbf{x} - \mathbf{W}\mathbf{x}) = \frac{1}{2} \mathbf{x}^T (\mathbf{I} - \mathbf{W})\mathbf{x},$$

which is exactly the graph Laplacian regularization. As we have shown in the analysis above, under the oracle setting, this does not have the noise rejection capability as PnP has.

• **Dynamics.** In this paper we assume that \mathbf{W} is defined through some pre-filtered signal, yet in practice \mathbf{W} is updated with the ADMM iterations. If \mathbf{W} is updated dynamically, obtaining a closed-form expression of the consensus equilibrium point would become very difficult. This is an open question, and more studies are needed to fully understand how to characterize the solution of this type.

• **Duality.** There is an interesting duality relationship between the graph Laplacian $(\mathbf{I} - \mathbf{W})$ and the PnP prior $(\mathbf{W}^{-1} - \mathbf{I})$. In fact, one can show that

$$(\mathbf{I} - \mathbf{W})^{-1} - (\mathbf{W}^{-1} - \mathbf{I})^{-1} = \mathbf{I}. \quad (63)$$

This result is reminiscent to one of the recent theoretical studies by Feizi et al [44] on generative adversarial network (GAN). The analogy is that if $(\mathbf{I} - \mathbf{W})$ represents a discriminator for the real data, then $(\mathbf{I} - \mathbf{W}^{-1})$ represents a discriminator for the generated data. It would be interesting to derive similar duality interpretation from a graph perspective.

• **Beyond Image Restoration.** Thus far we have exclusively discussed imaging applications. If we consider \mathbf{W} as a forward diffusion, then \mathbf{W}^{-1} is the reversal diffusion. It would be interesting to investigate applications in general graph domain.

VI. CONCLUSION

We presented an analysis to understand the performance of the PnP ADMM algorithm. The analysis is based on the class of graph filters. Our findings suggest a few reasons why PnP ADMM performs better than the conventional graph Laplacian regularization. From the direct mean squared error (MSE) perspective, the zero eigenvalues of the graph filter \mathbf{W} reject the noise of the observed signal before solving the inverse problem, whereas graph Laplacian retains the noise. As a result, the mean squared error of a PnP estimate has a lower variance than that of the graph Laplacian, and the drop in variance overrides the gain in bias, thus making the overall mean squared error lower.

To further understand the problem, we analyzed the performance from an equilibrium perspective. Instead of deriving

the solution from a MAP optimization, we derived the solution by inspecting the equilibrium condition of the ADMM subproblems. We showed that the PnP ADMM solution can be derived from multiple optimization formulations in which all give the same equilibrium solution.

As more sophisticated image restoration modules, e.g., deep neural networks, are being integrated into traditional model based recovery frameworks, we hypothesize that equilibrium will play an important role in analyzing the performance of these methods.

VII. ACKNOWLEDGEMENT

The author thanks Prof. Charles Bouman and Prof. Greg Buzzard of Purdue University for many inspiring discussions, Dr. Brendt Wohlberg of Los Alamos National Lab for offering valuable feedbacks on this paper, and Prof. Gene Cheung of York University for sharing thoughts on graph signal processing.

REFERENCES

- [1] S. Venkatakrisnan, C. Bouman, and B. Wohlberg, "Plug-and-Play priors for model based reconstruction," in *Proc. IEEE Global Conference on Signal and Information Processing*, 2013, pp. 945–948. 1
- [2] Y. Dar, A. M. Bruckstein, M. Elad, and R. Giryes, "Postprocessing of compressed images via sequential denoising," *IEEE Trans. Image Process.*, vol. 25, no. 7, pp. 3044–3058, Jul. 2016. 1
- [3] C. A. Metzler, A. Maleki, and R. G. Baraniuk, "From denoising to compressed sensing," *IEEE Trans. Information Theory*, vol. 62, no. 9, pp. 5117–5144, Sep. 2016. 1
- [4] A. Rond, R. Giryes, and M. Elad, "Poisson inverse problems by the Plug-and-Play scheme," *Journal of Visual Communication and Image Representation*, vol. 41, pp. 96–108, Nov. 2016. 1
- [5] U. S. Kamilov, H. Mansour, and B. Wohlberg, "A Plug-and-Play priors approach for solving nonlinear imaging inverse problems," *IEEE Signal Processing Letters*, vol. 24, no. 12, pp. 1872–1876, Dec 2017. 1
- [6] H. Chang and S. Marchesini, "A general framework for denoising phaseless diffraction measurements," Available online: <https://arxiv.org/abs/1611.01417>. 1
- [7] S. Ono, "Primal-dual Plug-and-Play image restoration," *IEEE Signal Processing Letters*, vol. 24, no. 8, pp. 1108–1112, Aug 2017. 1
- [8] S. Sreehari, S. V. Venkatakrisnan, B. Wohlberg, L. F. Drummy, J. P. Simmons, and C. A. Bouman, "Plug-and-Play priors for bright field electron tomography and sparse interpolation," *IEEE Trans. Computational Imaging*, vol. 2, no. 4, pp. 408–423, Dec. 2016. 1, 2, 3
- [9] S. H. Chan, X. Wang, and O. A. Elgandy, "Plug-and-Play ADMM for image restoration: Fixed point convergence and applications," *IEEE Trans. Computational Imaging*, vol. 3, no. 5, pp. 84–98, Mar. 2017. 1, 2, 4
- [10] A. M. Teodoro, J. M. Bioucas-Dias, and M. A. T. Figueiredo, "A convergent image fusion algorithm using scene-adapted gaussian-mixture-based denoising," *IEEE Trans. Image Processing*, vol. 28, no. 1, pp. 451–463, Jan 2019. 1, 2, 3, 4
- [11] F. Heide, M. Steinberger, Y.-T. Tsai, M. Rouf, D. Pajkak, D. Reddy, O. Gallo, J. Liu, W. Heidrich, K. Egiazarian, J. Kautz, and K. Pulli, "FlexISP: A flexible camera image processing framework," *ACM Trans. Graph.*, vol. 33, no. 6, pp. 231:1–231:13, Nov. 2014. 1
- [12] K. Zhang, W. Zuo, S. Gu, and L. Zhang, "Learning deep CNN denoiser prior for image restoration," in *Proc. IEEE Computer Society Conference on Computer Vision and Pattern Recognition (CVPR'17)*, July 2017, pp. 2808–2817. 1
- [13] K. Zhang, W. Zuo, Y. Chen, D. Meng, and L. Zhang, "Beyond a gaussian denoiser: Residual learning of deep CNN for image denoising," *IEEE Trans. Image Process.*, vol. 26, no. 7, pp. 3142–3155, July 2017. 1
- [14] M. Borgerding, P. Schniter, and S. Rangan, "AMP-inspired deep networks for sparse linear inverse problems," *IEEE Trans. Signal Process.*, vol. 65, no. 16, pp. 4293–4308, Aug 2017. 1
- [15] S. Boyd, N. Parikh, E. Chu, B. Peleato, and J. Eckstein, "Distributed optimization and statistical learning via the alternating direction method of multipliers," *Found. Trends Mach. Learn.*, vol. 3, no. 1, pp. 1–122, Jan. 2011. 1

- [16] E. T. Reehorst and P. Schniter, "Regularization by denoising: Clarifications and new interpretations," Available online: <https://arxiv.org/abs/1806.02296>. 2, 3, 12
- [17] Y. Romano, M. Elad, and P. Milanfar, "The little engine that could: Regularization by denoising (RED)," *SIAM Journal on Imaging Sciences*, vol. 10, no. 4, pp. 1804–1844, Oct. 2017. 2, 11
- [18] S. A. Bigdeli, M. Jin, P. Favaro, and M. Zwicker, "Deep mean-shift priors for image restoration," *Advances in Neural Information Processing Systems*, pp. 763–772, 2017. 2
- [19] T. Tírer and R. Giryes, "Image restoration by iterative denoising and backward projections," *IEEE Trans. Image Processing*, vol. 28, no. 3, pp. 1220–1234, Mar. 2019. 2
- [20] J. J. Moreau, "Proximité et dualité dans un espace hilbertien," *Bull. Société Mathématique France*, vol. 93, no. 3, pp. 273–299, 1965. 2, 3
- [21] S. H. Chan, "Algorithm-induced prior for image restoration," Available online at: <https://arxiv.org/abs/1602.00715>. 2, 4
- [22] G. T. Buzzard, S. H. Chan, S. Sreehari, and C. A. Bouman, "Plug-and-Play Unplugged: Optimization free reconstruction using consensus equilibrium," *SIAM Journal on Imaging Science*, vol. 11, no. 3, pp. 2001–2020, Sep. 2018. 2, 8
- [23] P. Milanfar, "A tour of modern image filtering," *IEEE Signal Process. Mag.*, vol. 30, pp. 106–128, Jan. 2013. 2
- [24] P. Milanfar, "Symmetrizing smoothing filters," *SIAM Journal on Imaging Sciences*, vol. 6, no. 1, pp. 263–284, Feb. 2013. 2
- [25] S. H. Chan, T. Zickler, and Y. M. Lu, "Understanding symmetric smoothing filters: A gaussian mixture model perspective," *IEEE Trans. Image Process.*, vol. 26, no. 11, pp. 5107–5121, Nov. 2017. 2
- [26] F. Meyer and X. Shen, "Perturbation of the eigenvectors of the graph Laplacian: Application to image denoising," *Applied and Computational Harmonic Analysis*, vol. 36, no. 2, pp. 326–334, Mar 2014. 2
- [27] H. Talebi, X. Zhu, and P. Milanfar, "How to SAIF-ly boost denoising performance," *IEEE Trans. Image Process.*, vol. 22, no. 4, pp. 1470–1485, Apr. 2013. 2
- [28] K. M. Taylor and F. G. Meyer, "A random walk on image patches," *SIAM Journal on Imaging Sciences*, vol. 5, pp. 688–725, 2012. 2
- [29] A. Kheradmand and P. Milanfar, "A general framework for regularized similarity-based image restoration," *IEEE Trans. Image Process.*, vol. 23, no. 12, pp. 5136–5151, Dec. 2014. 2, 9
- [30] H. Talebi and P. Milanfar, "Global image denoising," *IEEE Trans. Image Process.*, vol. 23, no. 2, pp. 755–768, Feb. 2014. 2, 11
- [31] J. Pang and G. Cheung, "Graph Laplacian regularization for image denoising: analysis in the continuous domain," *IEEE Trans. Image Process.*, vol. 26, no. 4, pp. 1770–1785, Apr. 2017. 2
- [32] Y. Bai, G. Cheung, X. Liu, and W. Gao, "Graph-based blind image deblurring from a single photograph," *IEEE Trans. Image Process.*, vol. 28, no. 3, pp. 1404–1418, Mar. 2019. 2
- [33] X. Liu, G. Cheung, X. Wu, and D. Zhao, "Random walk graph Laplacian-based smoothness prior for soft decoding of JPEG images," *IEEE Trans. Image Process.*, vol. 26, no. 2, pp. 509–524, Feb. 2017. 2
- [34] A. Anis, A. Gadde, and A. Ortega, "Efficient sampling set selection for bandlimited graph signals using graph spectral proxies," *IEEE Trans. Signal Process.*, vol. 64, no. 14, pp. 3775–3789, Jul. 2016. 2
- [35] N. Tremblay, P. Goncalves, and P. Borgnat, "Chapter 11 - design of graph filters and filterbanks," in *Cooperative and Graph Signal Processing*, pp. 299–324. Academic Press, 2018. 2
- [36] R. Sinkhorn and P. Knopp, "Concerning non-negative matrices and doubly-stochastic matrices," *Pacific Journal of Mathematics*, vol. 21, pp. 343 – 348, 1967. 2
- [37] Y. Romano and M. Elad, "Boosting of image denoising algorithms," *SIAM Journal on Imaging Sciences*, vol. 8, no. 2, pp. 1187–1219, 2015. 3
- [38] S. Kantorovitz, *Several real variables*, Springer, 2016. 3
- [39] R. A. Horn and C. R. Johnson, *Matrix analysis*, Cambridge University Press, 2nd edition, 2012. 5
- [40] A. Knutson and T. Tao, "Honeycombs and sums of Hermitian matrices," *Notices of the American Mathematical Society*, vol. 48, no. 2, pp. 175–186, Feb. 2001. 5
- [41] D. I. Shuman, S. K. Narang, P. Frossard, A. Ortega, and P. Vandergheynst, "The emerging field of signal processing on graphs: Extending high-dimensional data analysis to networks and other irregular domains," *IEEE Signal Process. Mag.*, vol. 30, no. 3, pp. 83–98, Apr. 2013. 5
- [42] J. Choi, O. A. Elgendy, and S. H. Chan, "Optimal combination of image denoisers," Available online: <https://arxiv.org/pdf/1711.06712.pdf>. 10
- [43] D. Shepard, "A two-dimensional interpolation function for irregularly-spaced data," in *Proc. ACM National Conference*, 1968, pp. 517–524. 11
- [44] S. Feizi, C. Suh, F. Xia, and D. Tse, "Understanding GANs: the LQG Setting," Available online: <https://arxiv.org/abs/1710.10793>. 12